# Fan Noise Source Diagnostic Test—Rotor Alone Aerodynamic Performance Results

Christopher E. Hughes, Robert J. Jeracki, Richard P. Woodward,
and Christopher J. Miller
Glenn Research Center, Cleveland, Ohio

April 2005

Since its founding, NASA has been dedicated to the advancement of aeronautics and space science. The NASA Scientific and Technical Information (STI) Program Office plays a key part in helping NASA maintain this important role.

The NASA STI Program Office is operated by Langley Research Center, the Lead Center for NASA's scientific and technical information. The NASA STI Program Office provides access to the NASA STI Database, the largest collection of aeronautical and space science STI in the world. The Program Office is also NASA's institutional mechanism for disseminating the results of its research and development activities. These results are published by NASA in the NASA STI Report Series, which includes the following report types:

- TECHNICAL PUBLICATION. Reports of completed research or a major significant phase of research that present the results of NASA programs and include extensive data or theoretical analysis. Includes compilations of significant scientific and technical data and information deemed to be of continuing reference value. NASA's counterpart of peer-reviewed formal professional papers but has less stringent limitations on manuscript length and extent of graphic presentations.

- TECHNICAL MEMORANDUM. Scientific and technical findings that are preliminary or of specialized interest, e.g., quick release reports, working papers, and bibliographies that contain minimal annotation. Does not contain extensive analysis.

- CONTRACTOR REPORT. Scientific and technical findings by NASA-sponsored contractors and grantees.

- CONFERENCE PUBLICATION. Collected papers from scientific and technical conferences, symposia, seminars, or other meetings sponsored or cosponsored by NASA.

- SPECIAL PUBLICATION. Scientific, technical, or historical information from NASA programs, projects, and missions, often concerned with subjects having substantial public interest.

- TECHNICAL TRANSLATION. English-language translations of foreign scientific and technical material pertinent to NASA's mission.

Specialized services that complement the STI Program Office's diverse offerings include creating custom thesauri, building customized data bases, organizing and publishing research results . . . even providing videos.

For more information about the NASA STI Program Office, see the following:

- Access the NASA STI Program Home Page at *http://www.sti.nasa.gov*

- E-mail your question via the Internet to help@sti.nasa.gov

- Fax your question to the NASA Access Help Desk at 301–621–0134

- Telephone the NASA Access Help Desk at 301–621–0390

- Write to:
  NASA Access Help Desk
  NASA Center for AeroSpace Information
  7121 Standard Drive
  Hanover, MD 21076

# Fan Noise Source Diagnostic Test—Rotor Alone Aerodynamic Performance Results

Christopher E. Hughes, Robert J. Jeracki, Richard P. Woodward,
and Christopher J. Miller
Glenn Research Center, Cleveland, Ohio

National Aeronautics and
Space Administration

Glenn Research Center

April 2005

## Acknowledgments

# Fan Noise Source Diagnostic Test—Rotor Alone
# Aerodynamic Performance Results

Christopher E. Hughes, Robert J. Jeracki, Richard P. Woodward, and Christopher J. Miller
National Aeronautics and Space Administration
Glenn Research Center
Cleveland, Ohio 44135

## Abstract

The aerodynamic performance of an isolated fan, or rotor alone, model was measured in the NASA Glenn Research Center 9- by 15-Foot Low Speed Wind Tunnel as part of the Fan Broadband Source Diagnostic Test conducted at NASA Glenn. The Source Diagnostic Test was conducted to identify the noise sources within a wind tunnel scale model of a turbofan engine and quantify their contribution to the overall system noise level. The fan was part of a 1/5th scale model representation of the bypass stage of a current technology turbofan engine. For the rotor alone testing, the fan and nacelle, including the inlet, external cowl and fixed area fan exit nozzle, were modeled in the test hardware; the internal outlet guide vanes located behind the fan were removed. Without the outlet guide vanes, the velocity at the nozzle exit changes significantly, thereby affecting the fan performance. As part of the investigation, variations in the fan nozzle area were tested in order to match as closely as possible the rotor alone performance with the fan performance obtained with the outlet guide vanes installed. The fan operating performance was determined using fixed pressure/temperature combination rakes and the corrected weight flow. The performance results indicate that a suitable nozzle exit was achieved to be able to closely match the rotor alone and fan/outlet guide vane configuration performance on the sea level operating line. A small shift in the slope of the sea level operating line was measured, which resulted in a slightly higher rotor alone fan pressure ratio at take-off conditions, matched fan performance at cutback conditions, and a slightly lower rotor alone fan pressure ratio at approach conditions. However, the small differences in fan performance at all fan conditions were considered too small to affect the fan acoustic performance.

## Introduction

Recent aircraft engine noise research by NASA and the aerospace industry[1-5] has focused on identifying the composition of the noise sources in a modern turbofan aircraft engine, their generation mechanisms, and the level of contribution to the total aircraft system noise level. A test was conducted in the NASA Glenn Research Center 9- by 15-Foot Low Speed Wind Tunnel (9x15 LSWT), called the Source Diagnostic Test. The objectives of the test were to investigate the aerodynamic and acoustic performance of the bypass stage portion of a scale model high bypass ratio turbofan engine and three Outlet Guide Vane (OGV) configurations that were designed to reduce turbofan noise. The turbofan model design was representative of a current technology high bypass turbofan engine in service today. As part of this test, detailed acoustic and aerodynamic flowfield surveys were conducted using a variety of research techniques. One of the techniques used to determine the fan only component of the system noise was eliminating the rotor/stator interaction by removing the OGVs. Since the OGVs are the structural supporting component for the model nacelle, an externally supported nacelle was used during testing. However, without the OGVs, the swirl component of the bypass nozzle exit flow was not removed, resulting in a higher fan exit velocity and lower fan exit pressure. Therefore, the fan nozzle exit area needed to be modified to produce the same fan operating conditions compared to a fan with OGVs installed at the same fan speed. This paper presents the process used in determining the correct nozzle exit area for the rotor alone nacelle, and compares the fan aerodynamic performance obtained without OGVs, or rotor alone performance, to the fan performance obtained with OGVs installed.

## Test Facilities

The 9x15 LSWT is a continuous flow, low turbulence, anechoic facility with flow velocity simulation capabilities from static to Mach number 0.23.[6] The wind tunnel test section is acoustically treated for conducting noise research and absorbs sound reflections down to 250 Hz.[7]

The fan model was driven by the NASA Glenn Ultra High Bypass (UHB) Drive Rig. The UHB Drive Rig is a propulsion simulator capable of generating up to 5,000 horsepower at shaft speeds up to 16,875 RPM using an air turbine driven by a high pressure, high temperature air supply.[8] A photograph of the fan model installed on the UHB Drive Rig in the 9x15 LSWT is shown in figure 1.

## Test Model Hardware

### Fan Module

The fan model used in the Source Diagnostic Test was a 1/5th scale model of a current technology turbofan engine. It was designed by General Electric Aircraft Engines (GEAE) under an internal research and development program, and was provided to NASA as part of a cooperative research effort for this test. The fan, referred to as the "R4" baseline fan, was 22 inches in diameter and had 22 blades. Its design stage pressure ratio was 1.47. Table 1 provides the design parameters for the R4 fan.

The three reduced noise OGV configurations were referred to as the Baseline, Low Count and Low Noise OGVs. The Baseline OGVs had 54 radial narrow chord vanes, the Low Count OGVs had 26 radial wide-chord vanes, and the Low Noise had 26 wide-chord vanes incorporating 30° of aft sweep. A schematic diagram of the fan and Baseline OGVs installed on the UHB Drive Rig is shown in figure 2, and a drawing illustrating the relationship of the fan and the three OGV configurations is shown in figure 3. The design geometries for the fan and the OGVs are given in table 2 for reference. A more detailed description of the design rationale for the R4 baseline fan and the reduced noise OGVs and their acoustic noise reduction benefit has been given by Envia, et al.,[9] Hughes,[2] and Woodward, et al.[3] The aerodynamic and farfield acoustic performance of the fan and each OGV configuration were measured over a range of fan operating conditions, including a sea level operating line representative of the performance with a fixed fan bypass nozzle exit area.[2,3]

### Rotor Alone Nacelle

To measure the fan alone contribution to the system noise level, a novel test technique was designed and developed by a team of research and system engineers at NASA Glenn.[10,11] This new test technique was referred to as the Rotor Alone Nacelle (RAN) system, and employed an isolated fan operating within an externally supported nacelle in the 9x15 LSWT. Photographs of the RAN installation in the 9x15 LSWT acoustic test section are shown in figure 4, and schematic diagrams of the installation are shown in figure 5.

The RAN system was comprised of the model turbofan nacelle and two aerodynamically shaped struts arranged in a bi-wing configuration to support the nacelle. The struts were located on the side of the nacelle opposite the traversing farfield acoustic microphone system, or the shadow side of the nacelle. In this way, any local noise sources associated with the airflow over the struts would be hidden from the farfield microphone field of view. A comparison of noise data obtained from an acoustic flow calibration test conducted in the 9x15 LSWT with the external nacelle support strut arrangement and the quietest fan/OGV configuration, the Low Noise OGVs, show that the external support struts had no effect on the overall model noise level.

The support struts connected the nacelle to an actuated, two-axis table system located outside the wind tunnel test section. As the fan speed increases, the fan thrust and power increase causing the UHB Drive Rig to move relative to the RAN. The tables were designed to reposition the nacelle vertically and horizontally in order to maintain a circumferentially uniform fan tip clearance with the nacelle over the entire fan operating envelope. Laser-based positioning sensors located in the nacelle determined the position of the nacelle with respect to the fan and UHB Drive Rig. The control system for the two-axis tables used the output from the laser sensors to determine the amount of position correction needed to keep the nacelle centered over the UHB Drive Rig, thereby centering the fan model within the nacelle. An illustration of the RAN nacelle and location of the laser sensors is shown in figure 6. Photographs showing the inside of the fan duct with a view of the laser sensor windows is shown in figure 7.

### Fan Nozzle

To achieve the proper rotor alone operating conditions, the fan nozzle exit area needed to be adjusted to compensate for the difference in the fan exit nozzle operating conditions. Without the OGVs present to straighten out the swirl induced into the

flow by the fan, the increase in the resultant nozzle exit velocity and the decrease in the nozzle exit pressure caused a shift in the fan operating line performance across the fan speed operating range. A quasi-2D flow analysis based on the conservation of mass and momentum was used to model the fan flow conditions from the inlet to the fan nozzle exit. The fan weight flow and average fan pressure rise and adiabatic efficiency were specified based on previous model experimental data. Between the fan and the OGVs, average flow conditions were calculated in both the axial and swirl directions. By adjusting the fan nozzle exit area to make the average exit static pressure match the free stream static pressure, the proper nozzle area was achieved, including the effect of the swirling flow. This technique used the proper nozzle exit total pressure, since no pressure loss from the OGVs was included. For this analysis, the discharge coefficient of the new, larger fan nozzle was assumed to be the same as the original nozzle.

Once the new fan nozzle exit area was established, a fan nozzle was fabricated and was made adjustable by allowing the exit area to be varied to allow for errors in the analysis that would affect the nozzle area calculation. The nozzle was made adjustable by adding 2 inches to its overall length. The inner and outer contours were designed with a convergent flowpath toward the fan nozzle exit, creating a positive pressure gradient on the flow surfaces. Therefore, as the fan nozzle length was shortened, the outer flowpath radius increased faster than the inner flowpath radius, thereby increasing the nozzle exit area.

*Modified External Model Configuration*

Since the swirl in the fan flow is not taken out during the rotor alone testing with no OGVs in the flow, there was concern that an additional noise source would be introduced as the swirling flow interacted with the UHB Drive Rig support strut located downstream of the fan model. Therefore, the fan flow exiting the nozzle and moving downstream along the UHB Drive Rig to the support strut was analyzed using the quasi-2D fan nozzle analysis for fan design point operating conditions (100 percent design speed) and static pressure data obtained on the model inner flowpath during initial rotor alone testing. Figure 8 shows the static pressure distribution on the inner flowpath for the 100 percent fan speed condition for both the rotor alone case and for the case with the Baseline OGVs installed in the model. For the

analysis, the total mass flow and angular momentum were held constant, the static pressure at the flow outer boundary was assumed to be the same as freestream static pressure, and the shear layer mixing effects at the outer jet boundary were ignored. Figure 9 illustrates the location of the flow property calculation planes with respect to the model. Figure 10 shows the analysis results. The Mach number distribution in the flow is shown in Figure 10a and the swirl angle distribution in the fan flow as a function of radius from the UHB Drive Rig centerline is shown in Figure 10b. In both figures, the outer radius of the flow streamtube was allowed to vary in order to get the right annular area to achieve the proper mass flow based on the inner flowpath static pressure. The analysis results indicate that as the flow moves downstream from the nozzle exit, the flow velocity increases significantly compared with the velocity distribution at the fan nozzle exit, especially toward the inner flowpath. Also, a swirl angle component persists as the fan flow moves downstream. These results indicated that there could indeed be contributing external noise contamination sources, both from the higher fan flow velocity and as the fan flow came into contact with the UHB Drive Rig strut at a high angle of attack.

Two modifications to the external model hardware configuration, then, were implemented to mitigate the introduction of additional noise. First, a constant area, cylindrical fairing was added to the inner flowpath in order to limit the increase in the flow velocity. The goal was to try and maintain the radial swirl angle and velocity distributions at a selected level downstream of the fan nozzle exit, at least to the UHB Drive Rig support strut. Figure 10a shows the predicted velocity distributions in the fan exit flow with a cylindrical, constant radius fairing added to the inner contour at a radius of 5.86". This radius was chosen for convenience because there is a model hardware flange located at model station 29.4, corresponding to this radius, on the inner flowpath, where the cylindrical fairing could be attached. From the figures, it can be seen that the velocity distribution in the fan flow at the RAN nozzle exit compared to the velocity distribution with the cylindrical fairing added are very close, in terms of their magnitudes. The difference is primarily the shift in the distribution radially because the inner flowpath radius is smaller where the cylindrical fairing starts compared to the fan nozzle exit. The constant radius fairing prevented the increase in velocity near the hub. Also, it can be seen that the predicted velocity distribution in the fan flow at the cylindrical fairing is close to the velocity distribution at the RAN fan nozzle exit.

Second, a leading edge fairing was added to the UHB Drive Rig support strut to try and turn the fan flow more axial before it came into contact with the strut, similar to an external turning vane. The radial length and turning angle distribution of the strut leading edge fairing design were obtained from the analytical prediction of rotor alone swirl angle, as seen in figure 10b, at the downstream model station where the leading edge fairing would be located. The predicted swirl angle distribution with the addition of the cylindrical centerbody fairing is shown in the figure. Except for a shift inboard to a lower radius, the predicted swirl angle distribution at the cylindrical fairing is relatively unchanged compared to the rotor alone fan nozzle exit. This is consistent with maintaining the total velocity distribution, which resulted from adding the cylindrical centerbody fairing.

Figure 11 shows photographs of the constant radius cylindrical fairing and the strut leading edge fairing installed on the UHB Drive Rig, respectively. Figure 12 gives two graphical representations of the strut leading edge fairing. In figure 13, the acoustic performance results of these RAN modifications are shown compared with the noise level of the fan and the quietest OGV configuration, the Low Noise OGVs. The results illustrate that the addition of the constant area cylindrical fairing on the model centerbody and the UHB Drive Rig strut leading edge fairing were successful in reducing the self-noise acoustics of the swirling, higher velocity fan flow. The fan flow self-noise was reduced up to 6 dB compared to the fan/OGV configuration. Also, the addition of the constant area cylindrical centerbody fairing and the UHB Drive Rig strut leading edge turning fairing reduced the self-noise of the fan flow compared with the original RAN inner flowpath configuration. Only at the highest fan speed at takeoff did the self-noise of the fan flow overcome the noise level of the fan/Low Noise OGV configuration, but by only 0.5 dB.

## Test Procedure

The fan performance on the acoustic operating line was first obtained with the OGVs installed. The procedure used for the fan performance testing has been described previously.[2] The fan module hardware configuration included the fixed area nozzle used for acoustic testing to obtain the correct fan operating line and a calibrated bellmouth inlet to measure the fan weight flow. The fan performance was measured using three fixed rakes mounted behind the fan. Each rake consisted of seven sensors, with each sensor comprised of a total pressure probe and total temperature probe co-located in an aspirated shield. The fan was operated over a range of speeds from 40 to 100.7 percent of the fan design speed. At each speed, the fan pressure and temperature rise were measured, as well as the freestream conditions in the test section.

For obtaining the rotor alone performance, the hardware configuration consisted of the RAN system (externally supported nacelle with laser-based position sensors, external support struts, translating tables and control system), bellmouth inlet and fan trim nozzle. The initial exit area for the RAN fan trim nozzle was intentionally set smaller than the predicted area required so that succeeding nozzle area adjustments would need to remove material from the nozzle length, increasing the fan nozzle exit area. The RAN fan performance results were compared with the fan/Baseline OGV performance results, and the fan trim nozzle exit area adjusted until the proper fan pressure ratio and fan weight flow were achieved. This process required three test runs resulting in three nozzle length adjustments to achieve the desired rotor alone operating line.

In figure 14, the sea level acoustic operating line performance of the fan with each of the three OGV configurations obtained by Hughes[2] are shown for reference. The rotor alone fan performance is compared with the fan/Baseline OGV performance on the sea level acoustic operating line. This figure illustrates that there was no measurable difference in the fan performance between the three OGV configurations, so the fan and Baseline OGVs can be used as an acceptable baseline for comparison with the rotor alone performance.

## Test Results

### *Fan Nozzle Area Variation*
The results of the RAN fan nozzle exit area trim testing are shown in figures 15 and 16. Figure 15 shows graphically the differences between original model inner and outer flowpath geometry contours and the final rotor alone flowpath contours including the trimmed fan exit nozzle. The inner and outer flowpath contours in the nacelle were modified from the original flowpath with OGVs for two reasons. First, a smoothed surface was created to fill in the regions where the OGV attachment points were

originally. And second, to control the radial velocity distributions internally and maintain the same velocity distributions compared with the OGVs as the flow moved axially downstream.

In figure 16, the fan performance results obtained during the fan nozzle exit area trim testing are shown. Figure 16a shows the corrected fan speed as a function of the corrected fan weight flow, and figure 16b shows the fan pressure ratio as a function of the corrected fan weight flow. The results show that as the fan nozzle exit area was increased, by shortening the nozzle length, the corrected fan weight flow went up and the fan pressure ratio went down at a given fan speed. For the initial full extension RAN fan nozzle, the fan weight flow and fan pressure ratio are significantly different than the final trimmed nozzle performance results. The fan nozzle exit area was initially set too small, since the corrected fan weight flow is low and the fan pressure ratio is high. Since the fan pressure ratio was significantly higher that desired, compared with the fan pressure ratio achieved with the OGVs installed, testing was stopped at the 70 percent corrected fan design speed point during the first nozzle trim test. Two additional adjustments were required to achieve the desired fan weight flow and fan pressure ratio across all fan speeds. Approximately 2.05 inches were removed from the fan nozzle length, resulting in a final RAN nozzle exit area of 236.1 in$^2$. The exit area of the fan nozzle used with the OGVs installed was 216.3 in$^2$.

### Sea Level Acoustic Operating Line Map

In figure 17, the RAN fan performance and the fan performance with the Baseline OGVs installed are compared on the sea level acoustic operating line. It can be seen in figures 17a to 17d, presenting the corrected fan weight flow, fan total pressure ratio, fan total temperature ratio and fan adiabatic efficiency results, respectively, that the RAN fan performance and the fan/Baseline OGV performance do not exactly lie on the same curve. There is a slight difference in the slope of the performance curves associated with the RAN and fan/Baseline OGV model configurations, causing a crossing of the curves in each of the performance plots. The trends in the performance results as well as the fan/Baseline OGV results, are consistent with the fan map performance results reported by Hughes.[2] As the fan weight flow is reduced by decreasing the fan nozzle exit area, the fan moves to a different operating point, and a different performance point, on a constant fan

speed line. The fan performance results in figure 17, for the given values of corrected fan weight flow and corrected fan speed, do lie on the fan maps for each fan speed line presented in Reference 2.

Based on the performance results, a compromise for the fan trim nozzle exit area was selected that minimized the differences in fan performance between the two configurations as a function of fan speed was necessary. The nominal cutback condition at 87.5 percent corrected fan speed was selected as the cross over point for the performance curves, and the RAN fan exit nozzle area was trimmed to achieve that cross over point as closely as possible. However, from the results, it can be seen in the figures that the fan speed cross over point is near 87.5 percent corrected fan speed, which is the cutback acoustic condition. Table 3 summarizes the RAN and fan/Baseline OGV performance measured at the three nominal acoustic rating points for this fan design—approach, cutback and takeoff (61.7, 87.5, and 100 percent corrected fan speed, respectively).

Figure 17a shows the corrected fan weight flow as a function of corrected fan speed. As can be seen, there are some small differences in the fan weight flow between the two model configurations. The largest difference is at the lower fan speeds. Near the design point, the RAN configuration shows a difference in fan weight flow approximately 0.55 percent lower than the fan/Baseline OGV configuration, indicating that the fan exit nozzle area is slightly smaller than desired. At the lower fan speeds, the opposite is true, with the RAN performance showing a slightly higher corrected fan weight flow, on the order of 1.3 percent.

Figure 17b shows the fan total pressure ratio results and figure 17c shows the fan total temperature ratio results for the RAN and fan/Baseline OGV test configurations. The results show a very small difference in total pressure ratio between the curves at the lower fan speeds, since at the lower speeds the total pressure ratio performance is fairly flat along the speed line. Near the design point at 100 percent corrected fan speed, the difference in performance is on the order of 0.13 percent, with the RAN curve showing the slightly higher total pressure rise. This is consistent with the corrected fan weight flow results in figure 17a, which indicated that the final trim nozzle exit area was slightly smaller than desired and driving the fan weight flow down.

The total temperature ratio results are presented in figure 17c and show performance trends with increases in fan speed and corrected fan weight flow similar to the total pressure ratio

results in figure 17b. Specifically, the RAN performance is slightly lower than the fan/Baseline OGV performance at corrected fan weight flows below the cross over point at 87.5 percent corrected fan speed, and slightly higher at corrected fan weight flows above the cross over point, because of the slightly smaller than desired final RAN fan nozzle exit area. The difference in total temperature ratio at the all fan speeds is small. At the fan design point at 100 percent corrected fan speed, the difference is about 0.10 percent, with the RAN performance slightly higher, which is the expected trend from the total pressure ratio and corrected fan weight flow results.

For the fan adiabatic efficiency, shown in figure 17d, the difference in the RAN and the fan/Baseline OGV performance is within 0.5 percent at all fan speeds above 55 percent corrected fan speed, corresponding to a corrected fan weight flow of about 52.5 lbs/sec. However, the difference is performance is smaller than that at most of the fan speed points tested. At fan speeds below the cross over point at cutback at 87.5 percent corrected fan speed, the RAN adiabatic efficiency is higher than the fan/OGV adiabatic efficiency. Above the cutback fan speed, the fan/OGV adiabatic efficiency is higher. Near the fan design point, the difference is about 0.44 percent, with the fan/Baseline OGV performance showing slightly higher performance than the RAN performance and at a slightly higher corrected fan weight flow. These results are also consistent with the fan performance maps in Reference 2. As the corrected fan weight flow drops with decreasing fan nozzle exit area, the fan adiabatic efficiency also drops along a constant fan speed line.

### Radial Profiles

In figure 18, the fan radial performance profiles for the RAN and fan/Baseline OGV configurations are compared for selected fan speeds. The total pressure ratio profiles are given in figure 18a and the total temperature ratio profiles are shown in figure 18b. The results indicate that at most fan speeds the radial distributions for the two configurations are very close to one another. Some small differences in fan performance are apparent near the fan tip, with larger differences appearing at the takeoff condition (100 percent corrected fan speed). The RAN performance results indicate that the fan tip is slightly under loaded but with a slightly higher temperature rise compared to the fan/Baseline OGV results. This may be due to a slight difference in the RAN fan tip clearance compared with the fan/Baseline OGV configuration. At the takeoff condition, the results clearly show a more significant variation in performance between the two configurations, with higher fan loading and lower temperature rise for the RAN configuration outboard from 50 percent span on the fan blade, with a difference of about 0.01 in fan pressure ratio. The results would indicate that the fan losses are slightly higher at the tip in the RAN configuration. Interestingly, the shape of the fan performance profiles are slightly different for the RAN configuration at takeoff, with a slight "knee" in the RAN results between 30 and 50 percent span that shows a slightly lower total pressure ratio compared with the fan/Baseline OGV results.

In figure 18c, the fan adiabatic efficiency results for the RAN and the fan/Baseline OGV configurations are shown for several fan speeds. The fan performance in the RAN configuration is higher at the lower fan speeds, while at the higher fan speeds the results show very little difference between the two configurations. The exception is near the fan tip, where the fan/Baseline OGV results shows a higher adiabatic efficiency than the RAN results for all fan speeds. Away from the fan tip, the largest differences in adiabatic efficiency are on the order of 1 percent at lower fan speeds, while the differences are near 2 percent at the tip at the fan design point. Figure 18d presents the same results as figure 18c except that adiabatic efficiency at the acoustic rating points fan speeds are shown for clarity.

## Summary and Conclusions

As part of the Fan Broadband Source Diagnostic Test, conducted in the NASA Glenn 9-by 15-Foot Low Speed Wind Tunnel, the feasibility of testing an isolated, scale model of the fan portion of a modern turbofan engine within a scale model engine nacelle was successfully demonstrated. The rotor alone wind tunnel model contained no internal outlet guide vanes behind the fan in order to identify and quantify the isolated fan, or rotor alone, noise sources in a turbofan engine. To reduce the self-noise of the swirling, high velocity fan flow exiting the RAN fan nozzle, a constant area cylindrical fairing was added to the model that effectively increased the diameter of the inner flowpath contour downstream of the fan nozzle. In addition, a turning vane was added to the UHB Drive Rig support strut leading edge to turn the swirling fan flow axially in order to reduce the angle of impingement of the fan flow on the strut. Both

these modifications were successful in reducing the fan flow self-noise up to 6 dB, depending on the fan speed condition, compared with the original, unmodified RAN and UHB Drive Rig hardware configurations.

The aerodynamic performance of the rotor alone was measured and compared with the performance of the fan with outlet guide vanes, or fan/OGV, configuration in support of the acoustic testing of the rotor alone configuration. This effort was necessary to ensure that the aerodynamic performance of the rotor alone configuration was very close to the performance of the fan/OGV configuration, allowing a valid acoustic comparison between the RAN and the fan/OGV configurations.

A comparison of the rotor alone configuration performance and the fan/OGV configuration performance shows that a fan exit nozzle area was experimentally obtained during this test for the rotor alone configuration that reasonably matched the fan/OGV configuration performance on the sea level acoustic operating line. Because of a different interaction of the swirling fan flow and the fixed area fan nozzle with fan speed, the acoustic operating line fan maps of the two configurations crossed over one another near the fan cutback condition at 87.5 percent of the corrected fan design speed. At fan speeds above cutback, the fan/OGV performance was slightly better than the rotor alone performance. The rotor alone total pressure ratio and total temperature ratio were slightly higher than the fan/OGV performance, while the corrected fan weight flow and adiabatic efficiency were lower. At takeoff, the difference in the corrected fan weight flow was 0.55 percent (fan/OGV higher), the total pressure ratio 0.13 percent (rotor alone higher) and the adiabatic efficiency about 0.5 percent (fan/OGV higher). Conversely, below cutback, the performance differences were reversed, with the rotor alone configuration showing slightly better performance than the fan/OGV performance. The largest differences between the fan configurations were at the lower speeds near approach conditions.

From the acoustic performance perspective, where matching the fan performance for these two model configurations was necessary in order to isolate and measure with reasonable accuracy the rotor alone contributions to the system noise, a rotor alone configuration for this scale model of the fan of a current technology high bypass turbofan was successfully modeled in the wind tunnel. The differences in performance between the rotor alone configuration and the fan configuration with outlet guide vanes that are presented in this report were considered small and would not significantly affect the overall fan noise level.

## References

1. Ganz, U., Joppa, P., Patten, J., Scharf, D., "Boeing 18-inch Fan Rig Broadband Noise Test," NASA/CR—1998-208704, 1998.
2. Hughes, C.E., "Aerodynamic Performance of Scale-Model Turbofan Outlet Guide Vanes Designed for Low Noise," NASA/TM—2001-211352, AIAA–2002–0374.
3. Woodward, R.P., and Hughes, C.E., "Fan Noise Source Diagnostic Test—Farfield Acoustic Results," AIAA–2002–2427.
4. Podboy, G.P., Krupar, M.J., Hughes, C.E., and Woodward, R.P., "Fan Noise Source Diagnostic Test—LDV Measured Flow Field Results," AIAA–2002–2431.
5. Podboy, G.P., Krupar, M.J., Helland, S.M., and Hughes, C.E., "Steady and Unsteady Flow Field Measurements Within a NASA 22 Inch Fan Model," AIAA–2002–1033.
6. Arrington, A.E., and Gonsalez, J.C., "Flow Quality Improvements in the NASA Lewis Research Center 9- by 15-Foot Low Speed Wind Tunnel," NASA CR–195439, 1995.
7. Dahl, M.D. and Woodward, R.P., "Acoustical Evaluation of the NASA Lewis 9- By 15-Foot Low Speed Wind Tunnel," NASA TP–3274, 1992.
8. Balan, C. and Hoff, G.E., "Propulsion Simulator for High Bypass Turbofan Performance Evaluation," SAE 931410, 1993.
9. Envia, E., and Nallasamy, M., "Design Selection and Analysis of a Swept and Leaned Stator Concept," NASA/TM—1998-208662, Journal of Sound and Vibration, vol. 228, pp. 793–836, 1999.
10. Cunningham, C.C., Thompson, W.K., Hughes, C.E., "Performance Optimization of a Rotor Alone Nacelle for Acoustic Fan Testing," NASA/TM—2000-210599, AIAA–2001–0164.
11. Shook, T.D., Hughes, C.E., Thompson, W.K., Tavernelli, P.F., Cunningham, C.C., Shah, A.R., "Design and Integration of a Rotor Alone Nacelle for Acoustic Fan Testing," NASA/TM—2001-210820, AIAA–2001–1058.

Table 1. Fan design parameters

| | |
|---|---|
| No. of Fan Blades | 22 |
| Fan Tip Diameter | 22 in |
| Radius Ratio | 0.30 |
| Corrected Tip Speed | 1,215 ft/sec |
| Corrected RPM | 12,657 |
| Corrected Fan Weight Flow | 100.5 lbm/sec |
| Specific Flow | 41.8 lbm/sec-ft$^2$ |
| Stage Pressure Ratio | 1.47 |
| Design Bypass Ratio | 8.85 |

Table 2.—Summary of fan and OGV airfoil geometries

| | Span Location | Fan | Baseline | Low Count | Low Noise |
|---|---|---|---|---|---|
| No. Blades/Vanes | | 22 | 54 | 26 | 26 |
| Aft Sweep, deg | | --- | 0 | 0 | 30 |
| Aspect Ratio | Pitchline | 2.00 | 3.51 | 1.67 | 1.67 |
| Chord, in | Pitchline | 3.61 | 1.57 | 3.26 | 3.26 |
| | | | | | |
| Solidity | Hub | | 2.25 | 2.40 | 2.47 |
| | Pitchline | 1.73 | 1.52 | 1.51 | 1.53 |
| | Tip | | 1.23 | 1.20 | 1.22 |
| | | | | | |
| Stagger, [1,2] deg | Hub | | 12.56 | 14.85 | 13.36 |
| | Pitchline | 37.10 | 10.29 | 10.68 | 10.75 |
| | Tip | | 10.65 | 10.58 | 11.68 |
| | | | | | |
| Vane Camber, deg | Hub | --- | 38.40 | 44.20 | 45.47 |
| | Pitchline | --- | 34.56 | 37.57 | 36.06 |
| | Tip | --- | 40.49 | 43.00 | 39.16 |
| | | | | | |
| $t_{max}/c$ | Hub | 0.081 | 0.0707 | 0.0707 | 0.0638 |
| | Pitchline | 0.040 | 0.0702 | 0.0702 | 0.0640 |
| | Tip | 0.028 | 0.0698 | 0.0698 | 0.0639 |

[1] Defined from axial plane; positive angle in direction of fan rotation.
[2] Positive angle in opposite direction of fan rotation for OGVs.

Table 3.—Summary of Fan Performance

| Fan Operating Condition | Corrected Weight Flow, lb$_m$/sec | | Total Pressure Ratio | | Total Temperature Ratio | | Adiabatic Efficiency | |
|---|---|---|---|---|---|---|---|---|
| | RAN | Fan/OGV | RAN | Fan/OGV | RAN | Fan/OGV | RAN | Fan/OGV |
| Approach (61.7%) | 59.04 | 58.30 | 1.158 | 1.159 | 1.048 | 1.049 | 0.8909 | 0.8880 |
| Cutback (87.5%) | 83.92 | 83.91 | 1.359 | 1.360 | 1.102 | 1.102 | 0.9010 | 0.9020 |
| Takeoff (100%) | 96.65 | 97.18 | 1.511 | 1.509 | 1.138 | 1.136 | 0.9092 | 0.9136 |

Figure 1.—Source Diagnostic Test Fan Model installed in the
NASA Glenn 9- by 15-Foot Low Speed Wind Tunnel.
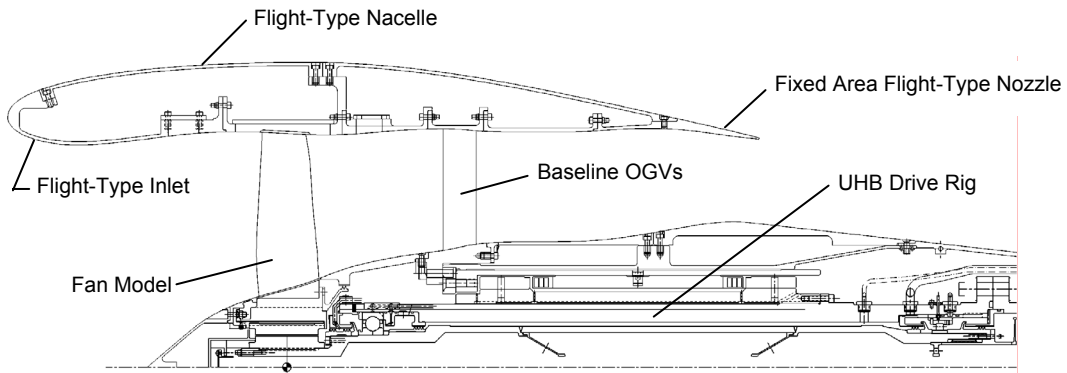


Figure 2.—Schematic diagram of the Fan Model and Baseline OGVs installed on the UHB Drive Rig.
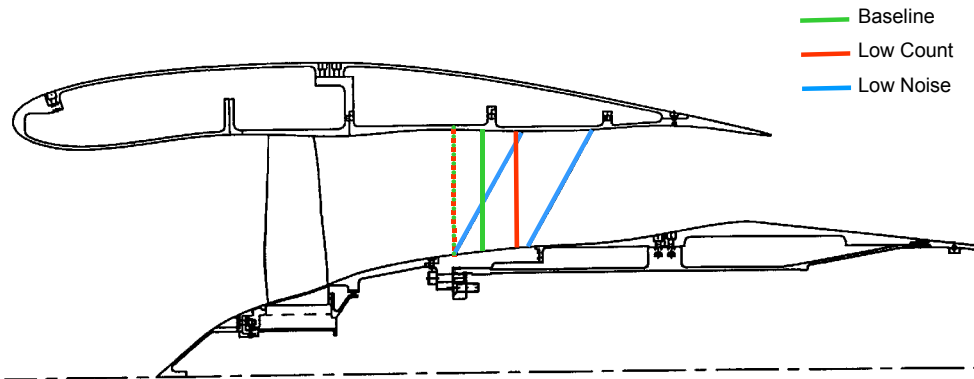


Figure 3.—Illustration showing the relationship of the fan and three OGV configurations.
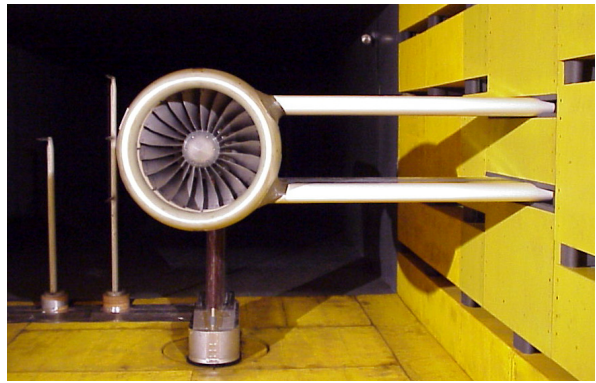
a. Left front view                                    b. Full front view, forward looking downstream

Figure 4.—Photographs of the Rotor Alone Nacelle installed in the 9x15 LSWT.



Externally Supported Nacelle

UHB Drive Rig

Fan Model

External Support Struts (2)

Test Section Wall

Two-Axis Translating Tables

a. Top view.



Test Section Acoustic Boxes

External Support Struts (2)

External Supported Nacelle

Translating Tables

Fan Model Centerbody

Drive Rig Support Strut
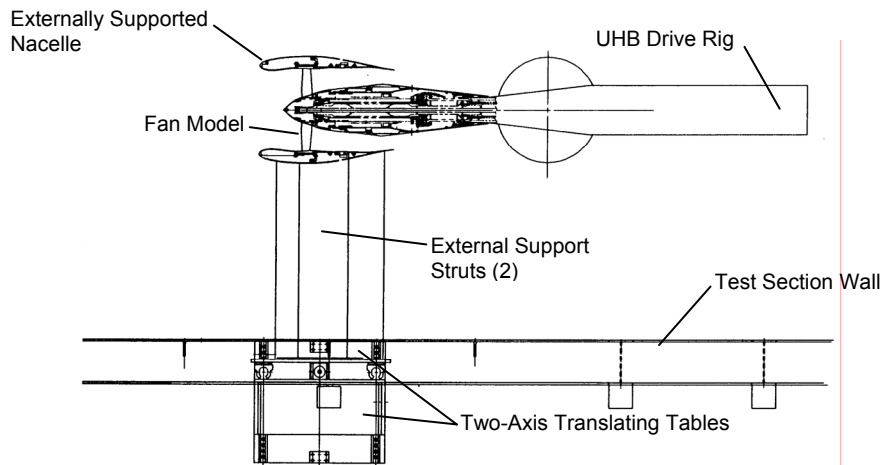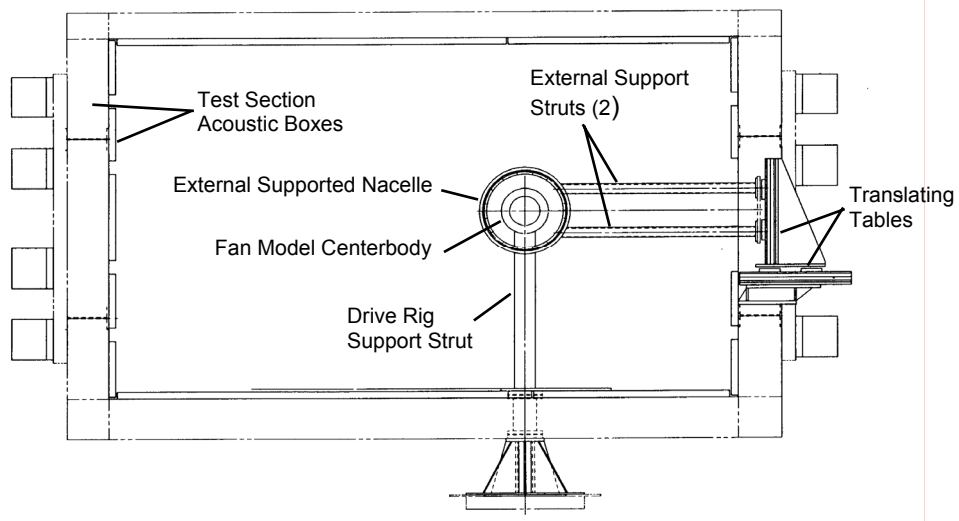
Figure 5.—Illustrations of the Rotor Alone Nacelle, external struts
and two-axis translating table installed in the 9x15 LSWT.
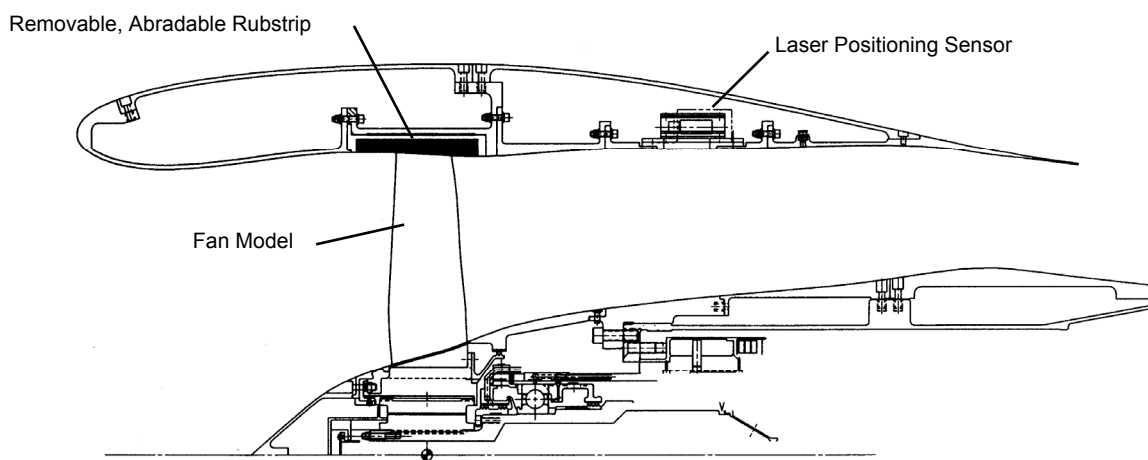
Figure 6.—Details schematic of the Rotor Alone Nacelle.
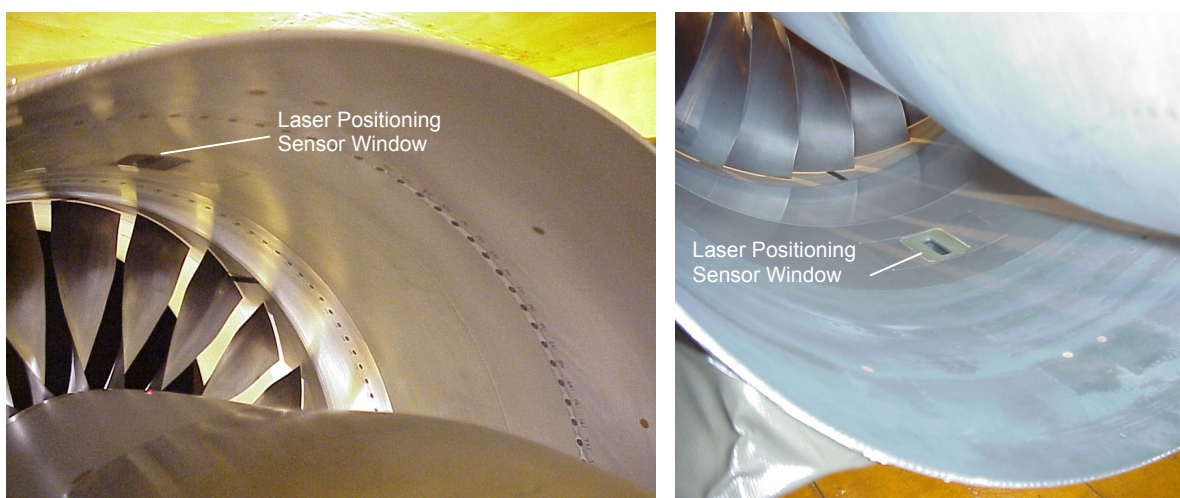


Figure 7.—Photographs inside the Rotor Alone Nacelle, from the nozzle looking upstream to the fan, showing the laser positioning sensor windows and illustrating the lack of OGVs.
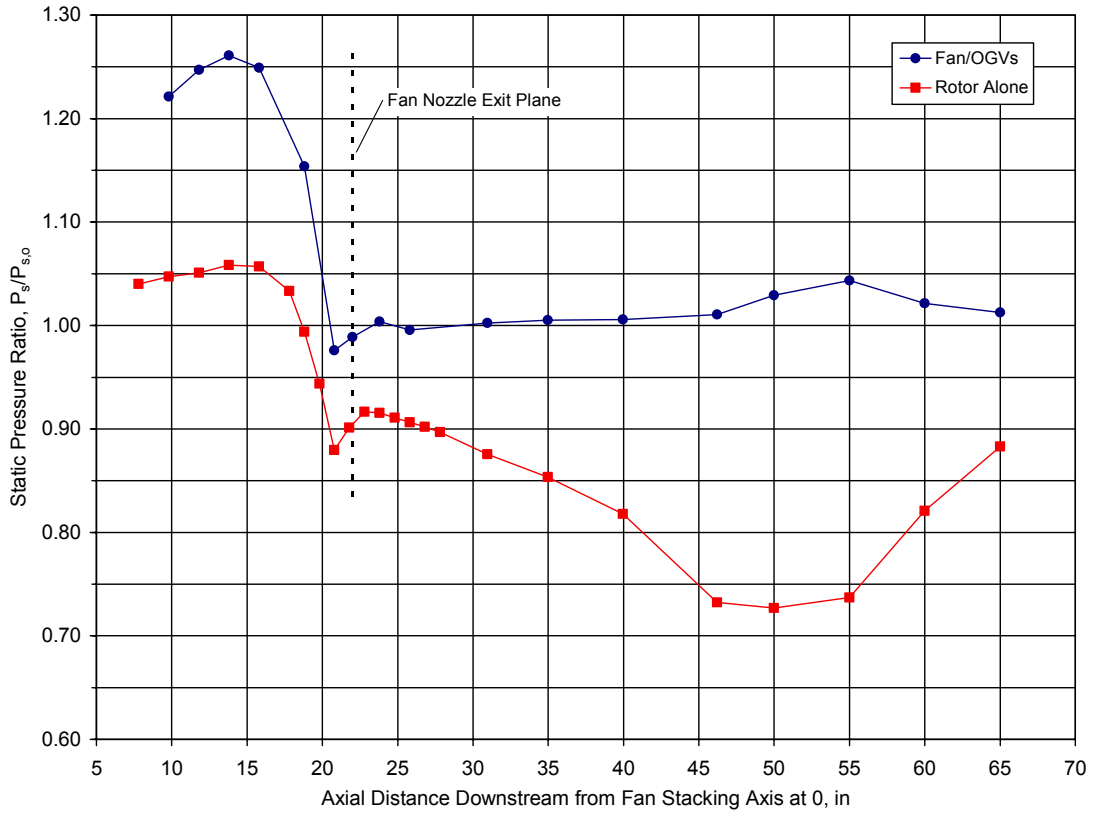
Figure 8.—Static pressure distribution on fan model inner flowpath for RAN
and fan/Baseline OGV configurations.
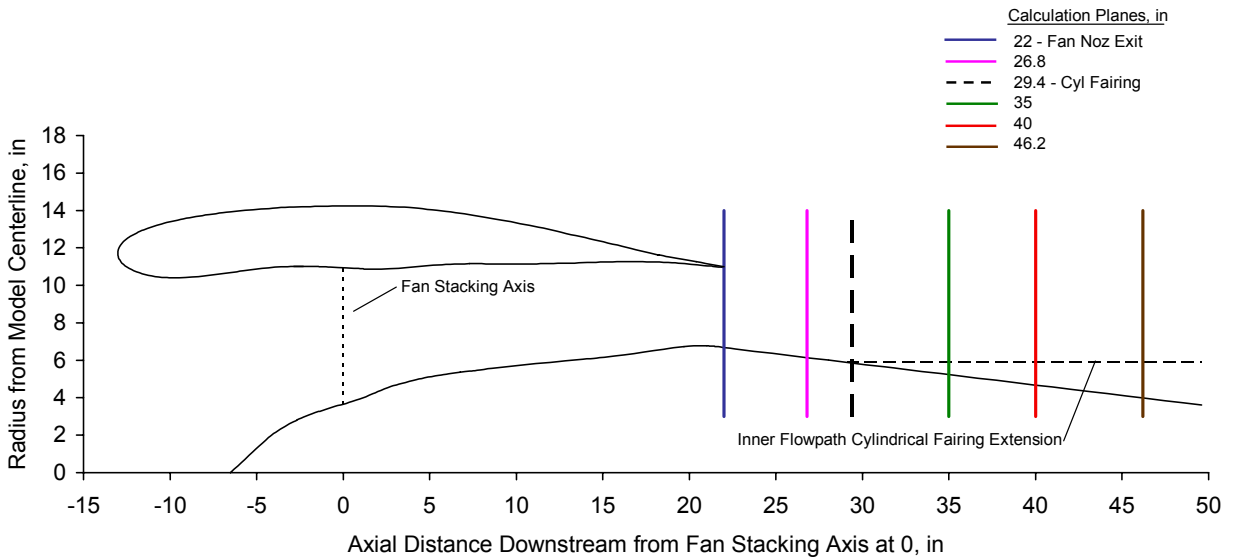


Figure 9.—Location of flow property calculation planes with respect to model geometry.
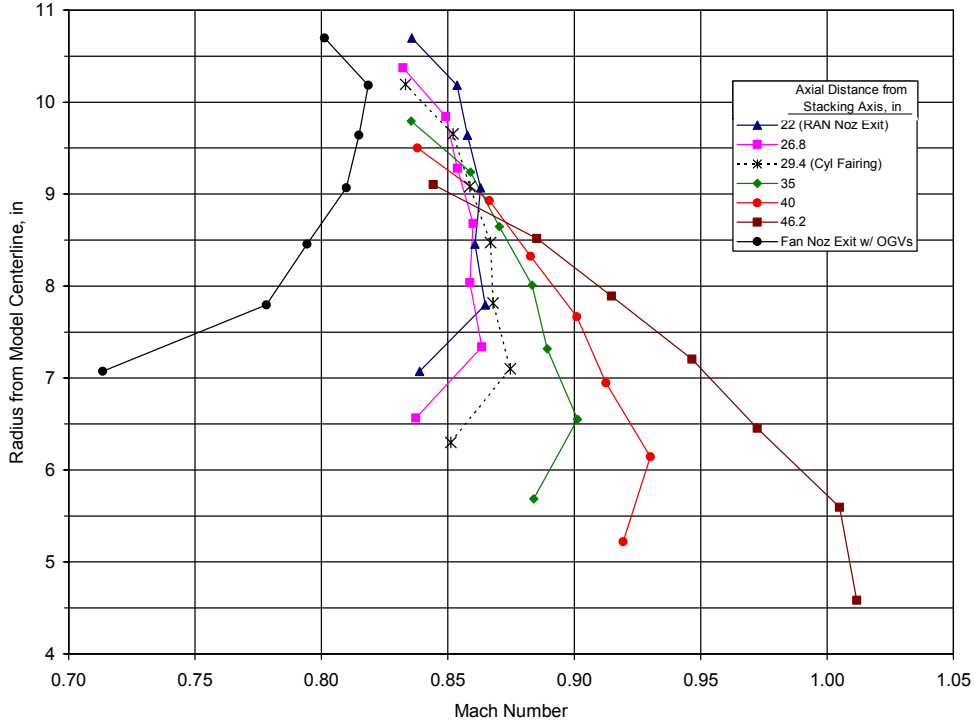
a. Radial swirl angle distribution in the RAN fan flow downstream of the fan nozzle exit
and with the addition of the constant area cylindrical fairing
on the inner flowpath downstream of the nozzle exit.
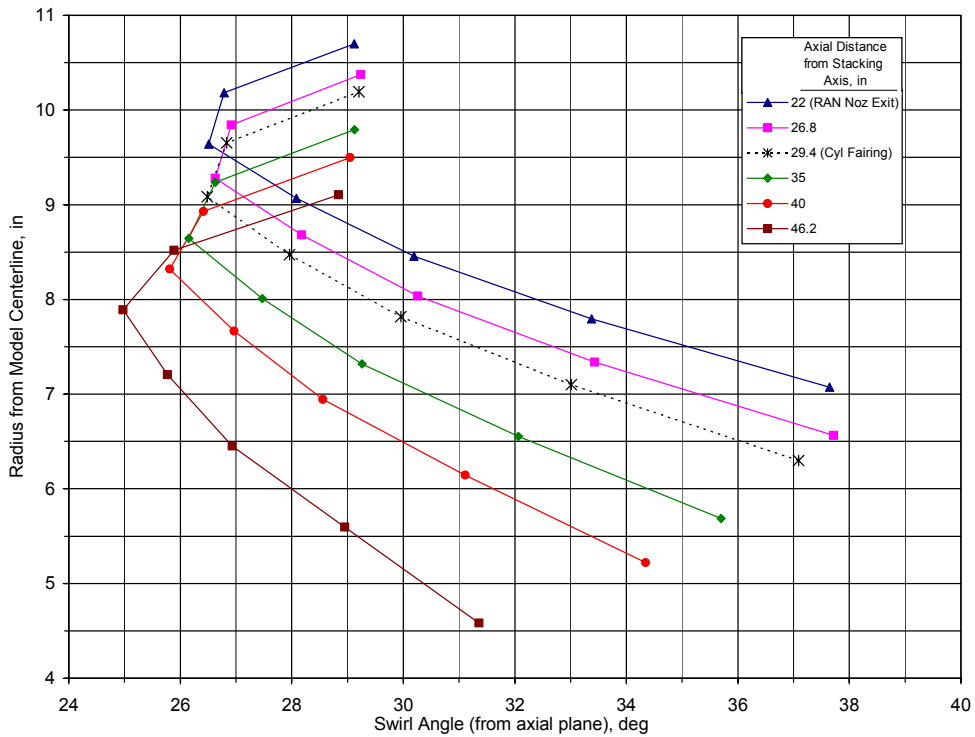


b. Radial velocity distribution in the fan flow downstream of the RAN fan nozzle exit and with the
addition of the constant area cylindrical fairing on the inner flowpath downstream of the nozzle exit.

Figure 10.—Calculation results of flow properties downstream of RAN fan nozzle exit.
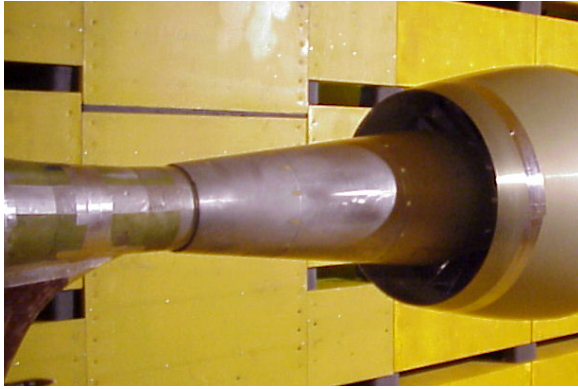
a. Original inner flowpath model hardware.



b. Constant area cylindrical fairing on inner flowpath.



c. Aft looking forward view of Rotor Alone Nacelle,
cylindrical fairing and UHB Drive Rig
strut leading edge fairing.
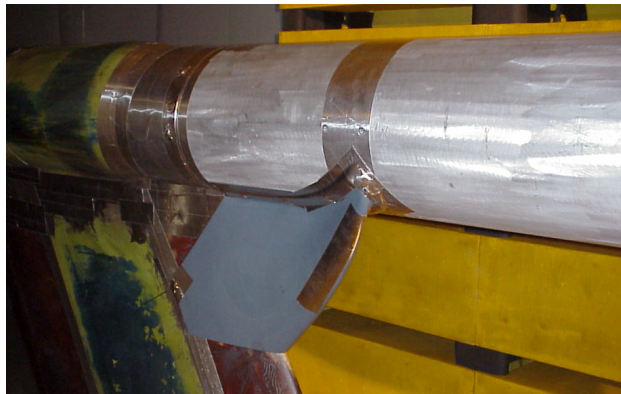


d. Close up view of strut leading edge fairing.
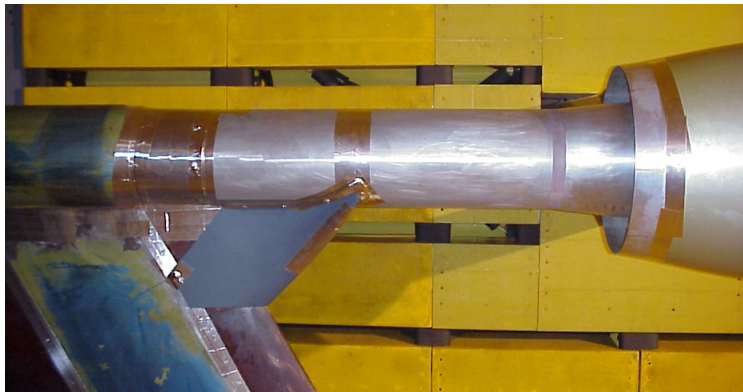


e. Side view of inner flowpath cylindrical fairing
and UHB Drive Rig strut leading edge fairing.

Figure 11.—Photographs of the flowpath modifications made to the
Rotor Alone Nacelle fan module configuration.

a. Front view, forward looking aft.

b. View looking up and aft from tunnel floor.
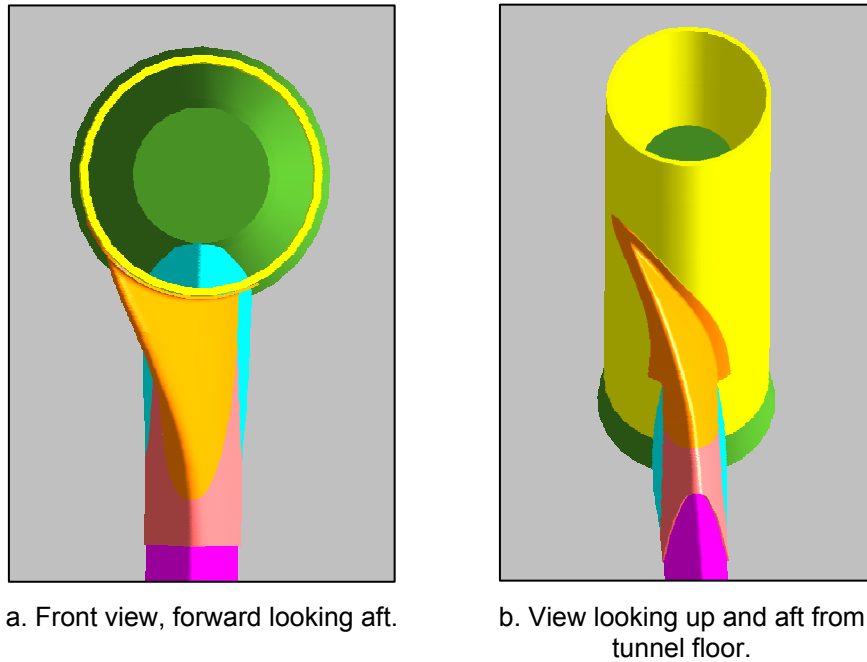
Figure 12.—Graphical representations of UHB Drive Rig support strut leading edge fairing illustrating the turning angle distribution.
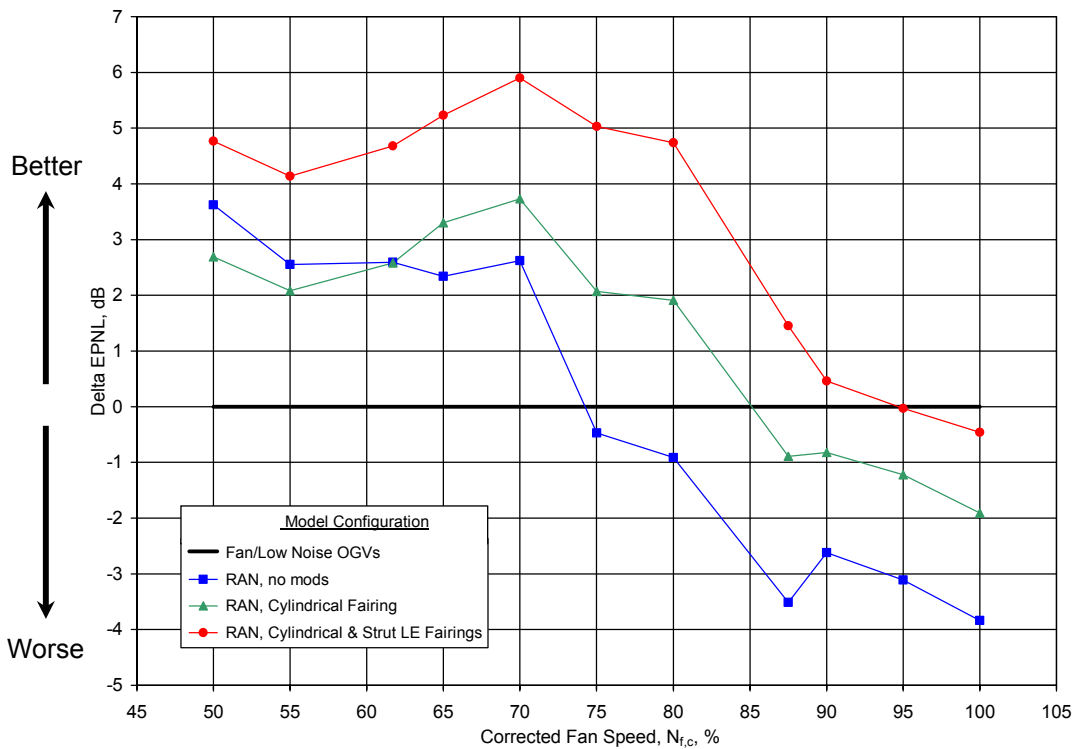


Figure 13.—Comparison of acoustic performance of the RAN hardware configurations with the addition of hardware modifications to reduce the fan flow self-noise.
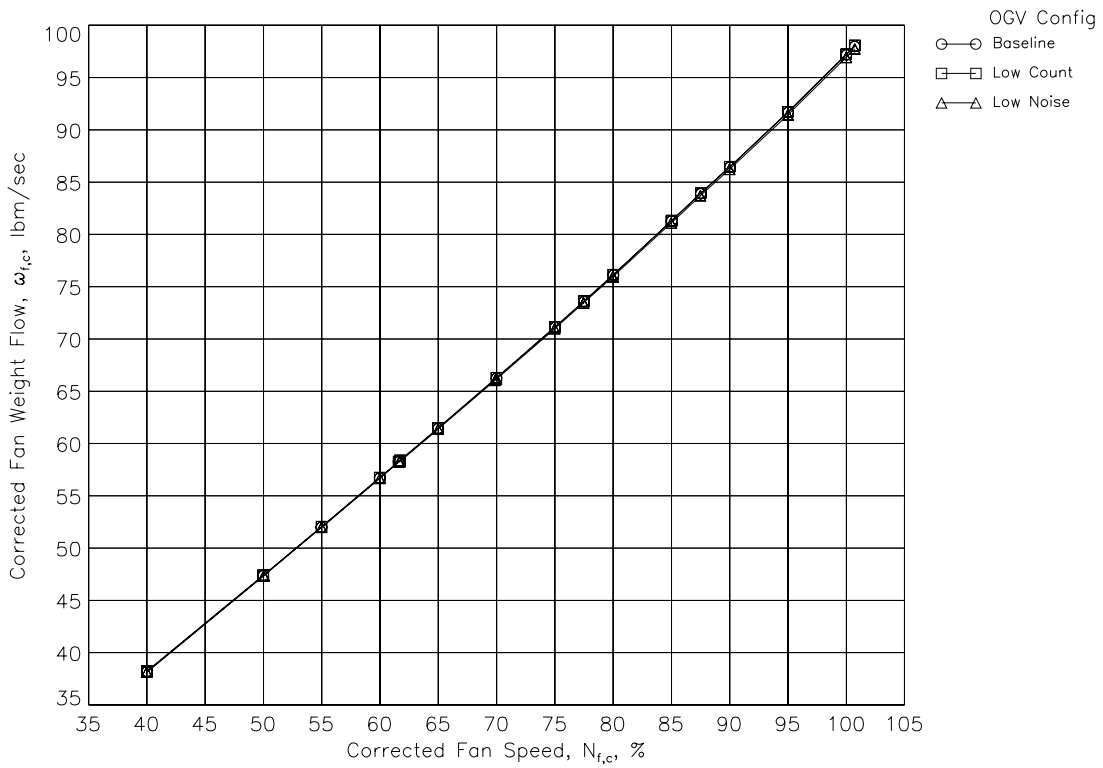
a. Fan corrected weight flow.
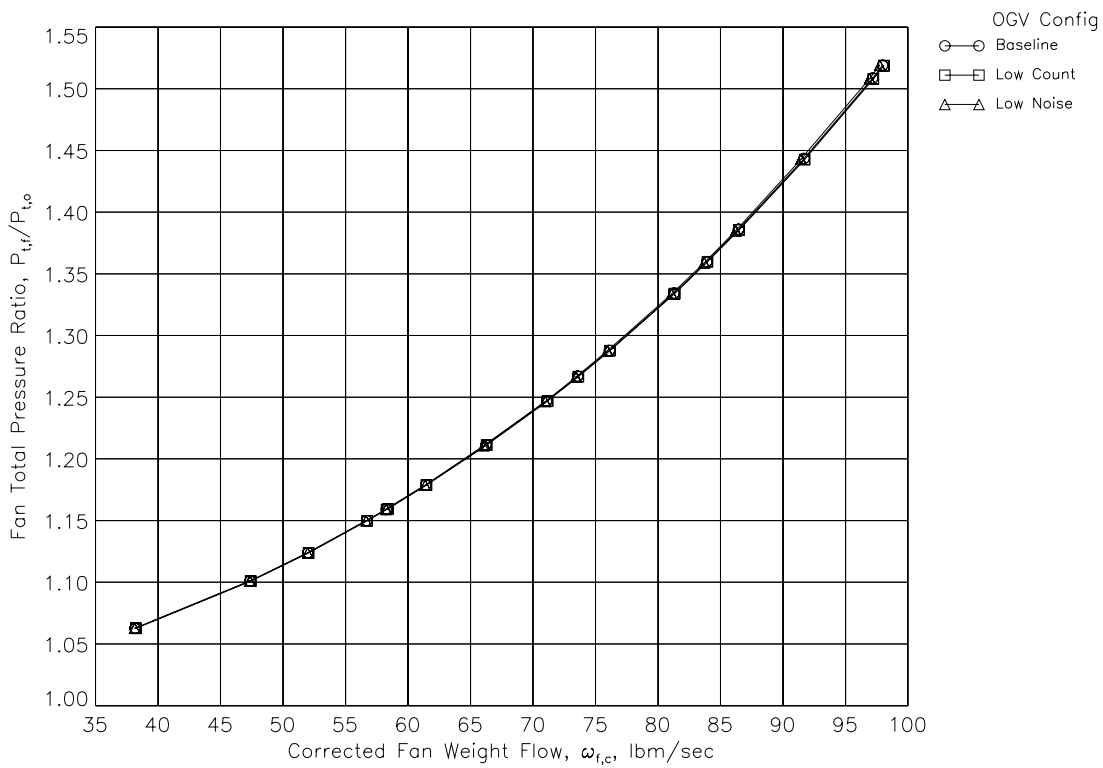


b. Fan total pressure ratio.

Figure 14.—Comparison of the fan performance with three different OGV configurations (continued).
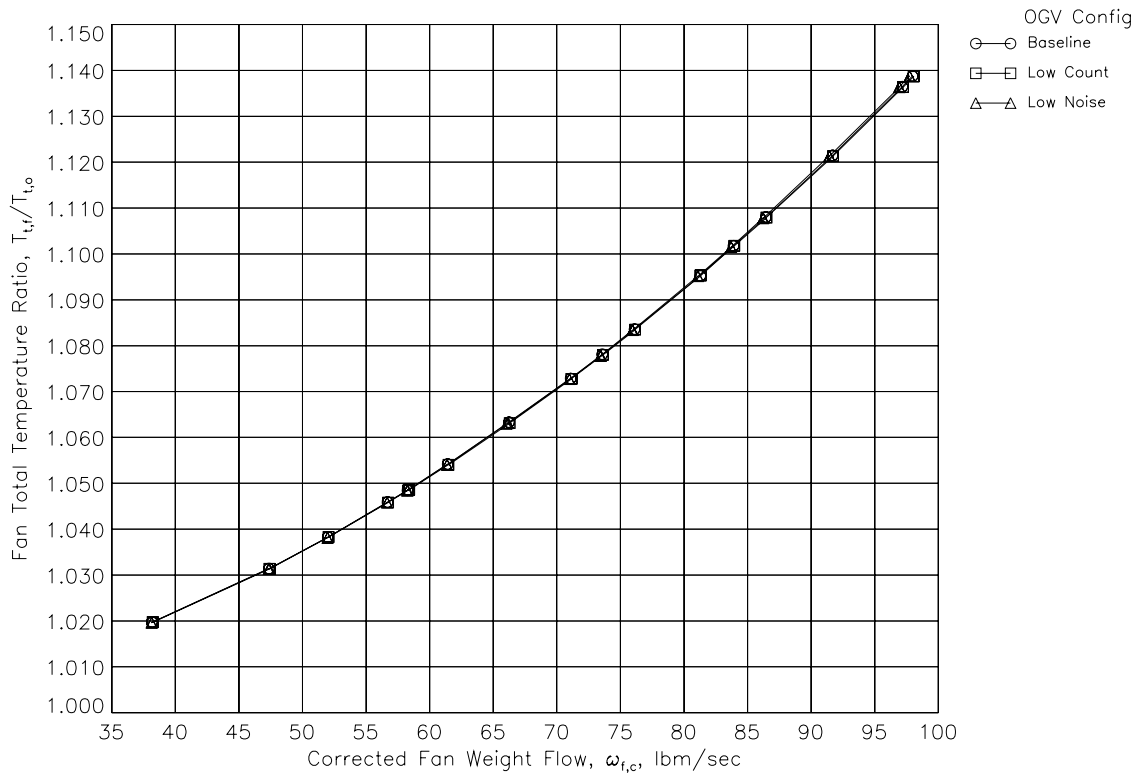
c. Fan total temperature ratio.
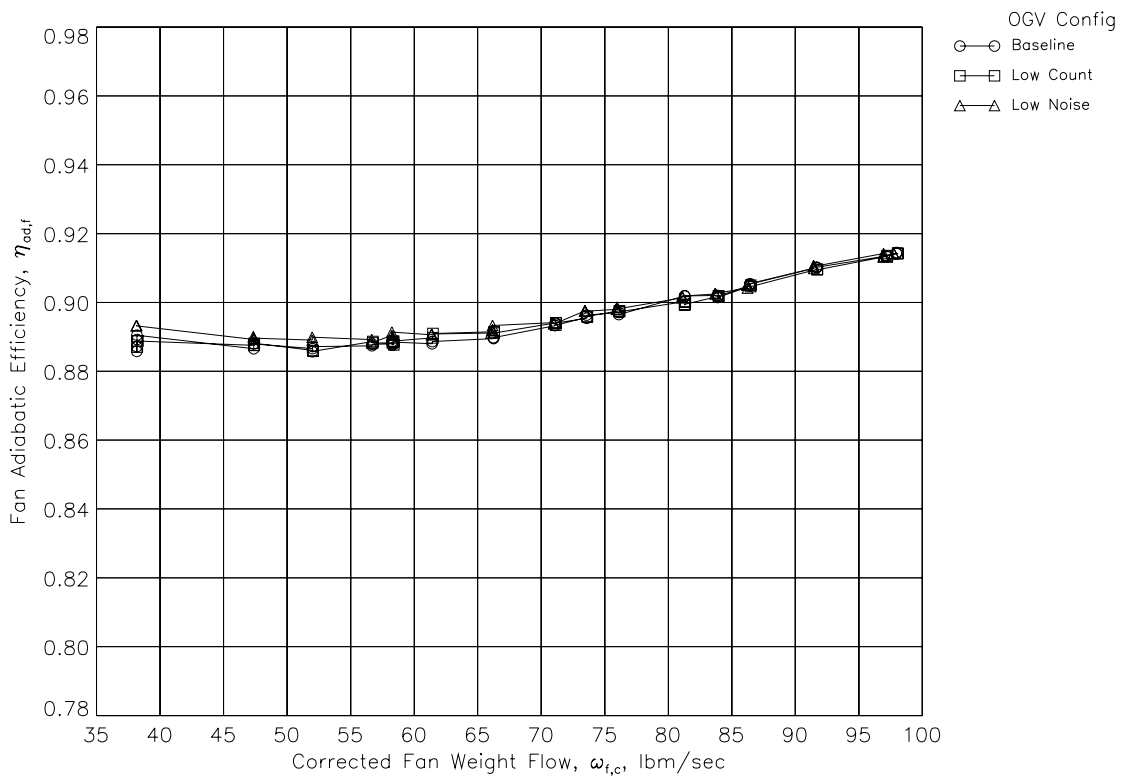


d. Fan adiabatic efficiency.

Figure 14.—Comparison of the fan performance with three different OGV configurations (concluded).
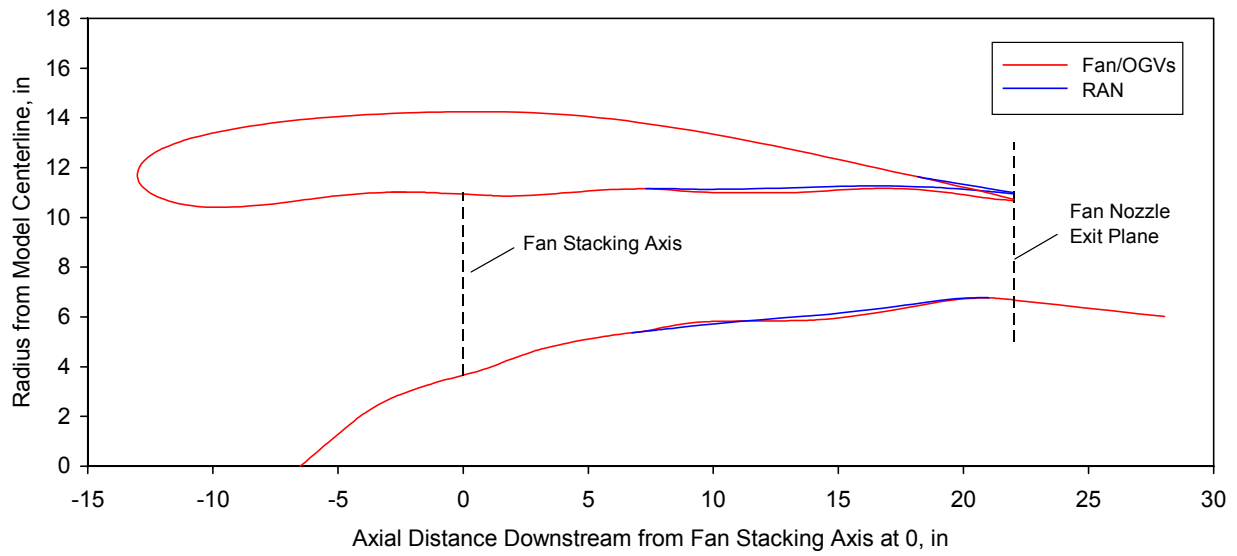
Figure 15.—Comparison of model inner and outer flowpath geometry with OGVs and the RAN geometry.
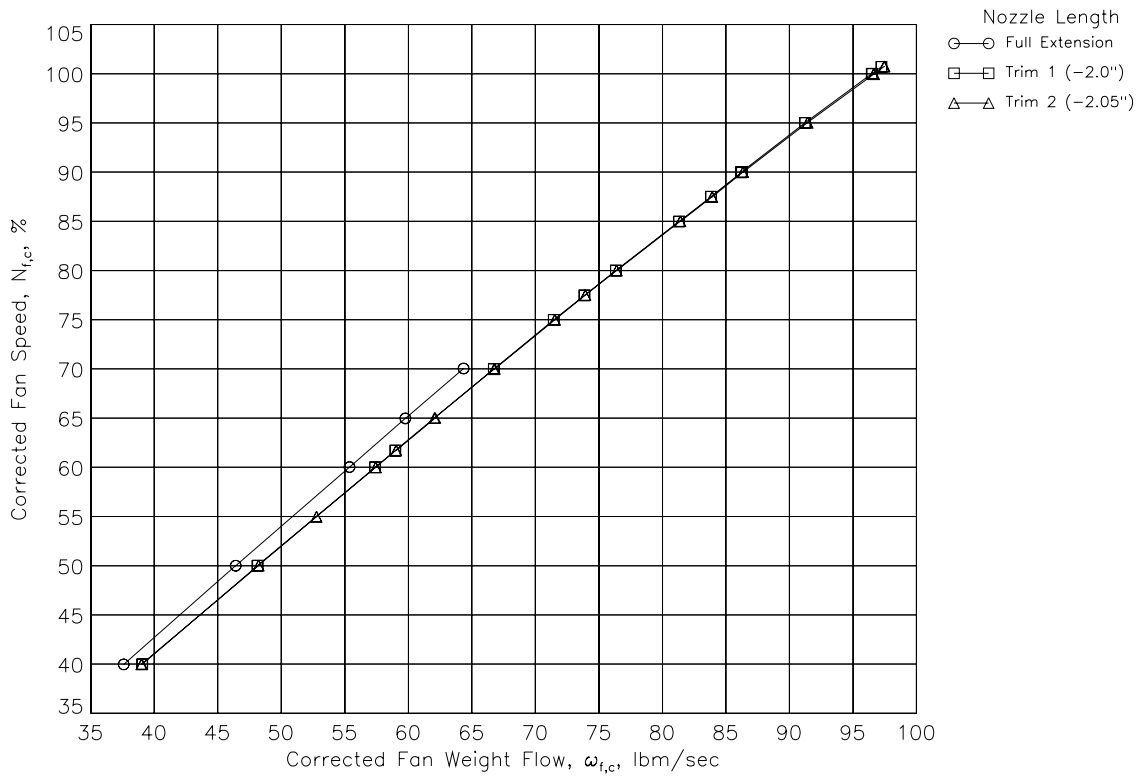
a. Corrected fan weight flow.
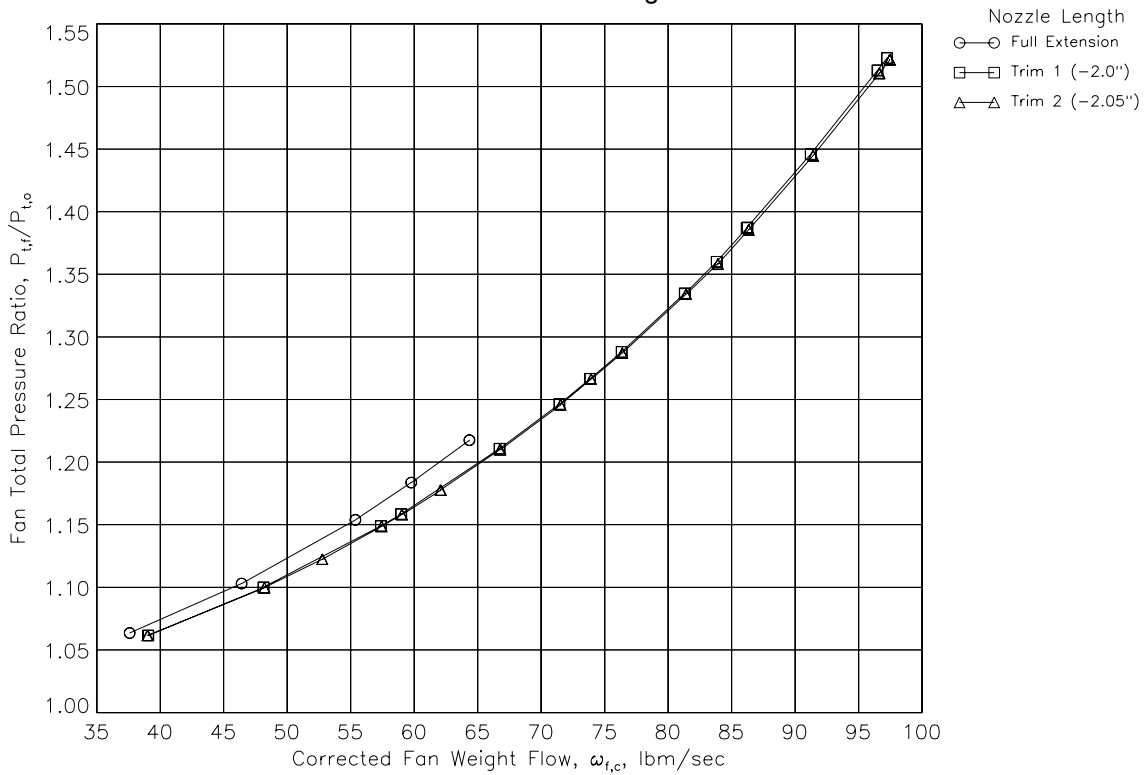


b. Fan total pressure ratio.

Figure 16.—Fan performance measurements during RAN fan exit nozzle trim testing to obtain the proper nozzle exit area.
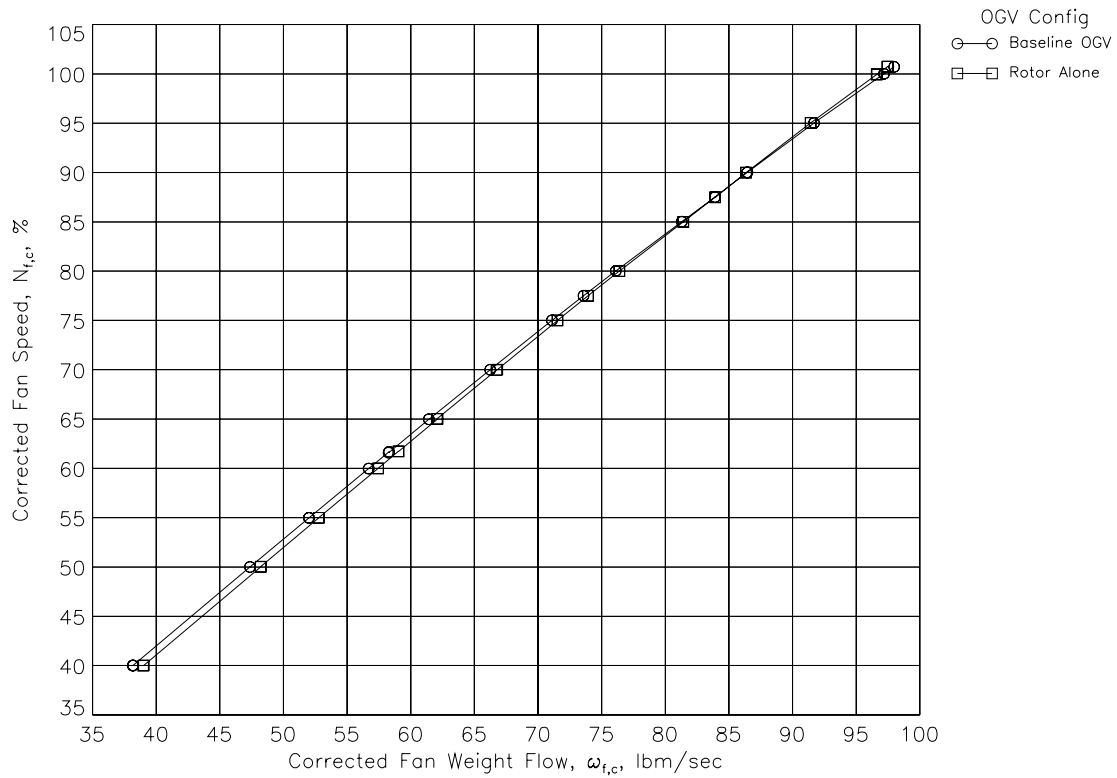
a. Corrected fan weight flow.
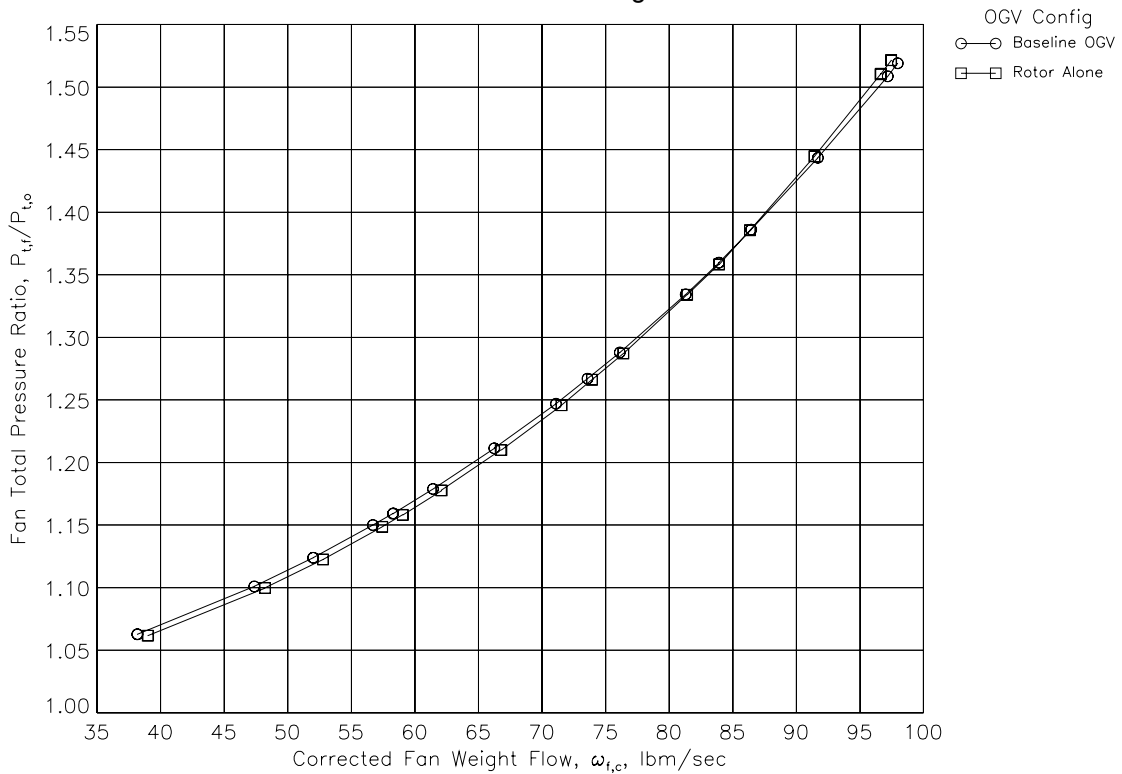


b. Fan total pressure ratio.

Figure 17.—Comparison of the fan aerodynamic performance on the acoustic operating line with Baseline OGVs installed and rotor alone with the final nozzle area (continued).
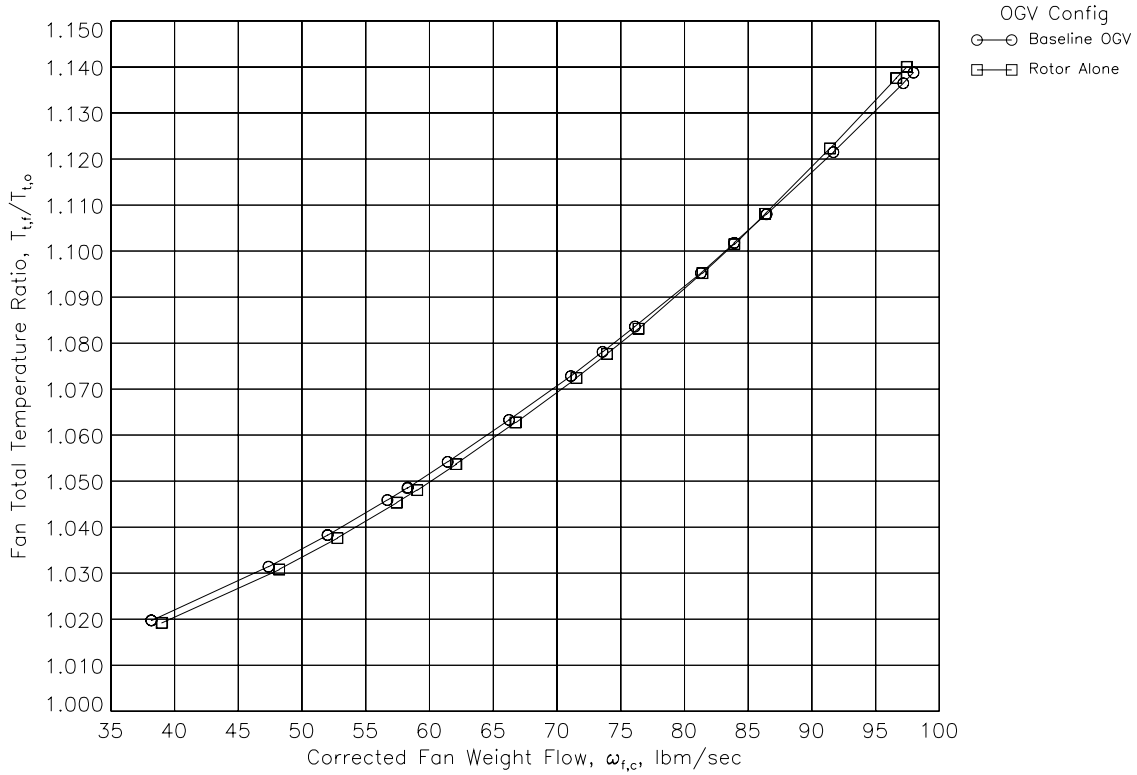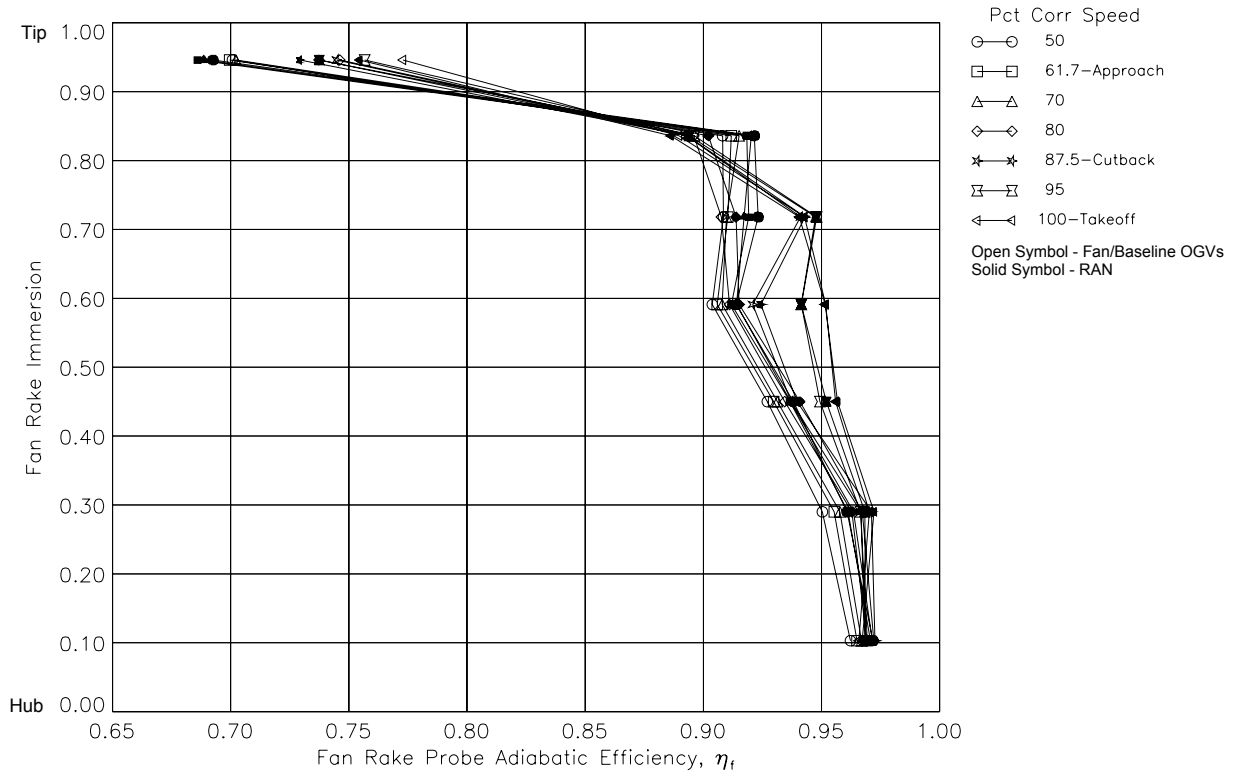
c. Fan total temperature ratio.
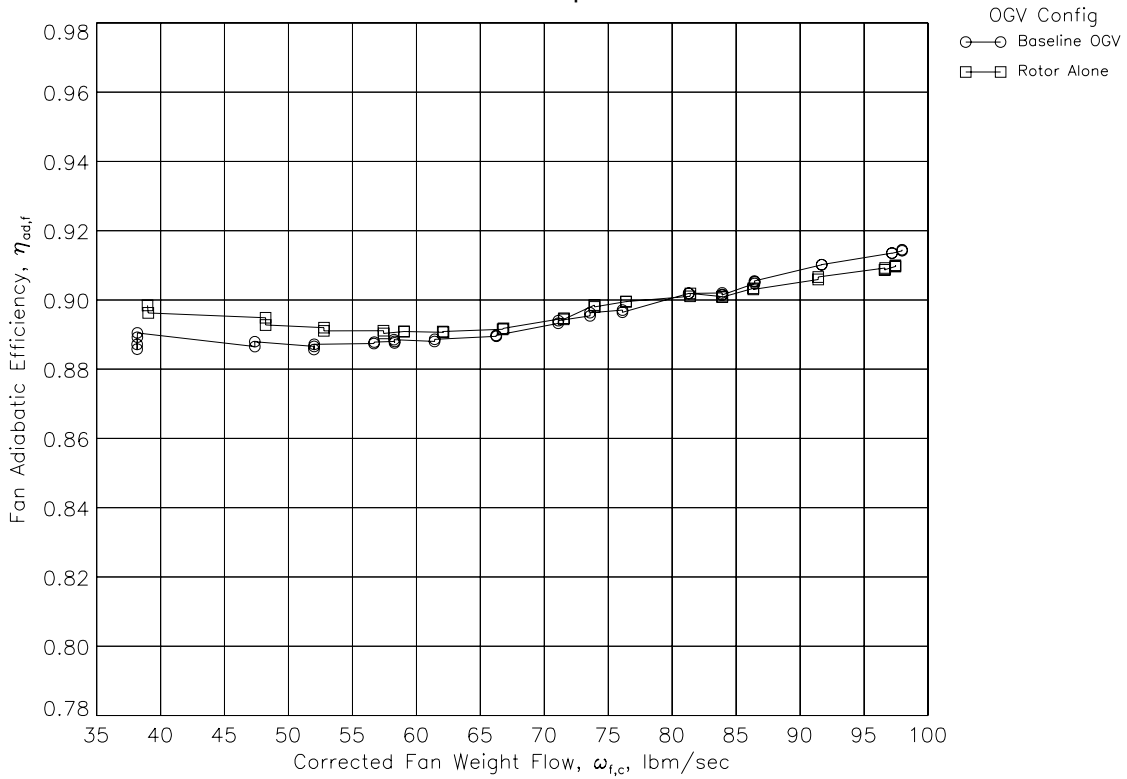


d. Fan adiabatic efficiency.

Figure 17.—Comparison of the fan aerodynamic performance on the acoustic operating line with Baseline OGVs installed and rotor alone with the final fan exit nozzle area (concluded).
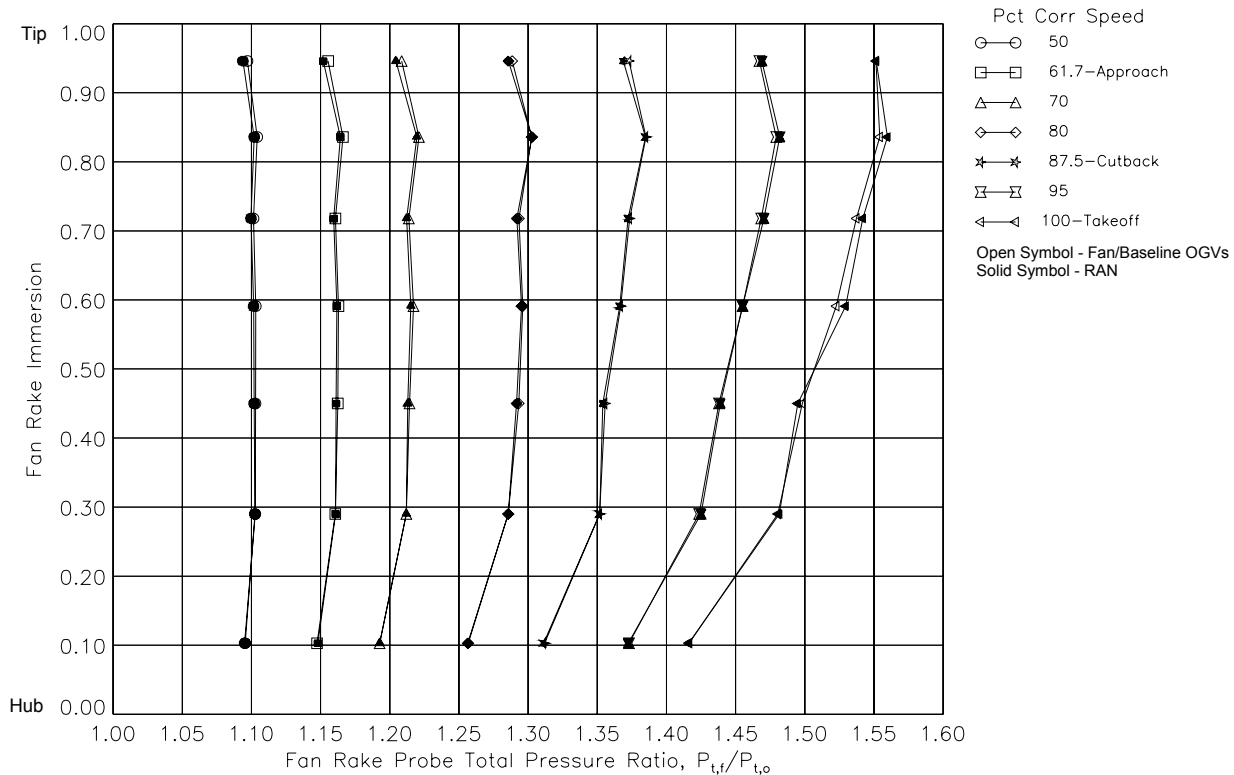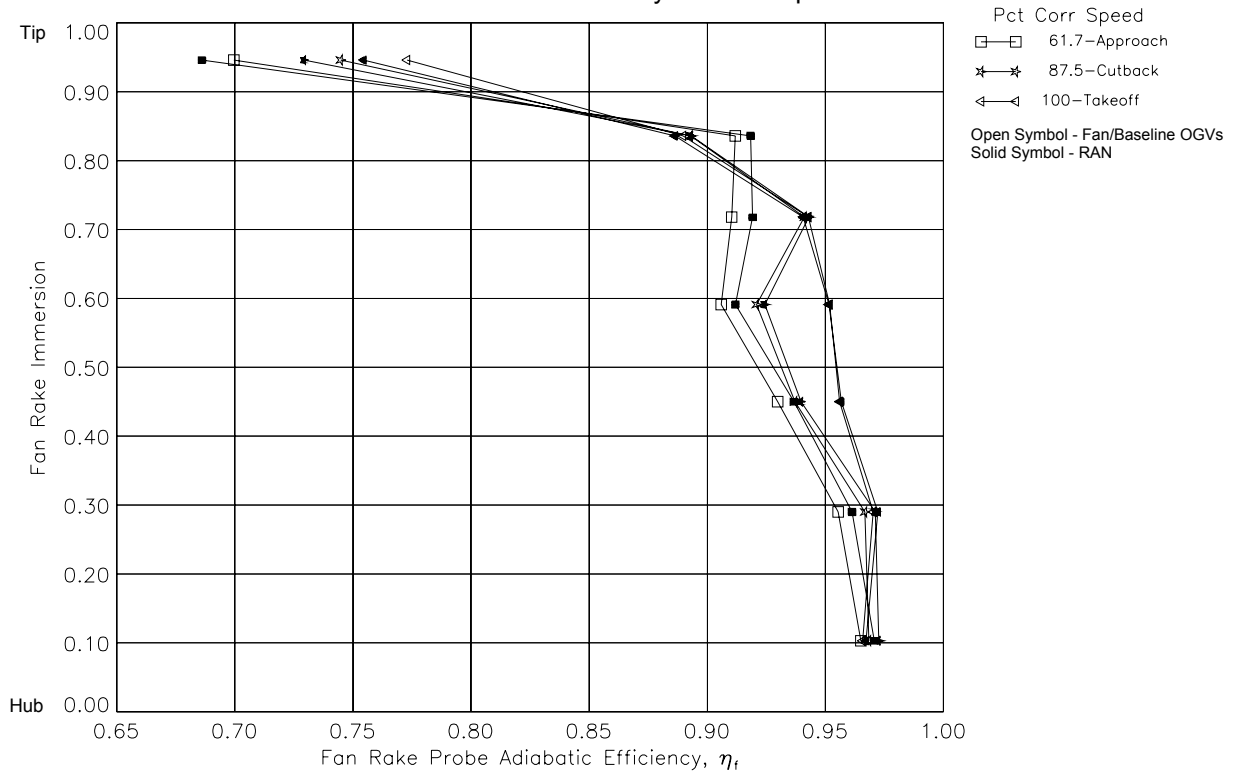
a. Fan total pressure ratio.
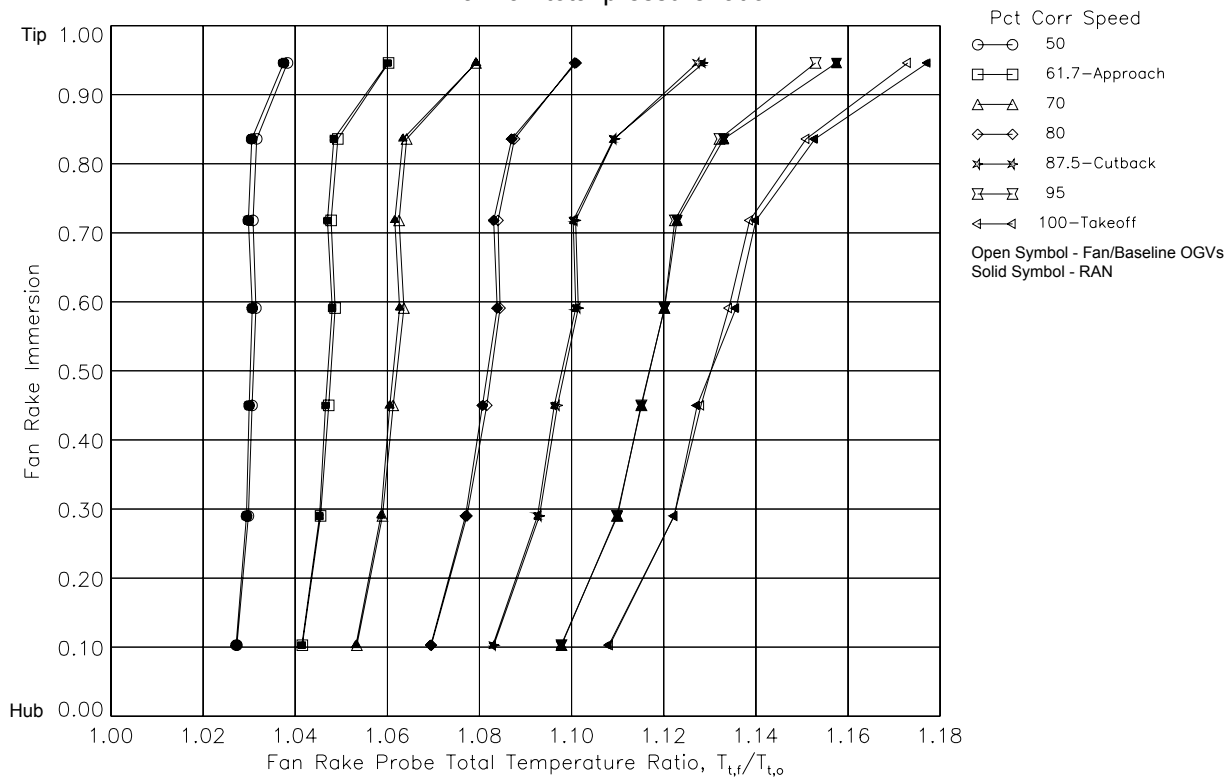


b. Fan total temperature ratio.

Figure 18.—Comparison of the fan rake radial performance profiles on the acoustic operating line with Baseline OGVs installed and rotor alone with the final nozzle area (continued).

c. Fan adiabatic efficiency at all fan speeds.



d. Fan adiabatic efficiency at the acoustic rating point fan speeds.

Figure 18.—Comparison of the fan rake radial performance profiles on the acoustic operating line with Baseline OGVs installed and rotor alone with the final nozzle area (concluded).

# REPORT DOCUMENTATION PAGE

| 1. AGENCY USE ONLY (Leave blank) | 2. REPORT DATE | 3. REPORT TYPE AND DATES COVERED |
|---|---|---|
| | April 2005 | Technical Memorandum |

**4. TITLE AND SUBTITLE**

Fan Noise Source Diagnostic Test—Rotor Alone Aerodynamic Performance Results

**5. FUNDING NUMBERS**

WBS–22–781–30–74

**6. AUTHOR(S)**

Christopher E. Hughes, Robert J. Jeracki, Richard P. Woodward, and Christopher J. Miller

**7. PERFORMING ORGANIZATION NAME(S) AND ADDRESS(ES)**

National Aeronautics and Space Administration
John H. Glenn Research Center at Lewis Field
Cleveland, Ohio 44135–3191

**8. PERFORMING ORGANIZATION REPORT NUMBER**

E–13384

**9. SPONSORING/MONITORING AGENCY NAME(S) AND ADDRESS(ES)**

National Aeronautics and Space Administration
Washington, DC 20546–0001

**10. SPONSORING/MONITORING AGENCY REPORT NUMBER**

NASA TM—2005-211681
AIAA–2002–2426

**11. SUPPLEMENTARY NOTES**

**12a. DISTRIBUTION/AVAILABILITY STATEMENT**

Unclassified - Unlimited
Subject Category: 02          Distribution: Nonstandard

Available electronically at http://gltrs.grc.nasa.gov/GLTRS

This publication is available from the NASA Center for AeroSpace Information, 301–621–0390.

**12b. DISTRIBUTION CODE**

**13. ABSTRACT (Maximum 200 words)**

The aerodynamic performance of an isolated fan or rotor alone model was measured in the NASA Glenn Research Center 9- by 15-Foot Low Speed Wind Tunnel as part of the Fan Broadband Source Diagnostic Test conducted at NASA Glenn. The Source Diagnostic Test was conducted to identify the noise sources within a wind tunnel scale model of a turbofan engine and quantify their contribution to the overall system noise level. The fan was part of a 1/5th scale model representation of the bypass stage of a current technology turbofan engine. For the rotor alone testing, the fan and nacelle, including the inlet, external cowl, and fixed area fan exit nozzle, were modeled in the test hardware; the internal outlet guide vanes located behind the fan were removed. Without the outlet guide vanes, the velocity at the nozzle exit changes significantly, thereby affecting the fan performance. As part of the investigation, variations in the fan nozzle area were tested in order to match as closely as possible the rotor alone performance with the fan performance obtained with the outlet guide vanes installed. The fan operating performance was determined using fixed pressure/temperature combination rakes and the corrected weight flow. The performance results indicate that a suitable nozzle exit was achieved to be able to closely match the rotor alone and fan/outlet guide vane configuration performance on the sea level operating line. A small shift in the slope of the sea level operating line was measured, which resulted in a slightly higher rotor alone fan pressure ratio at take-off conditions, matched fan performance at cutback conditions, and a slightly lower rotor alone fan pressure ratio at approach conditions. However, the small differences in fan performance at all fan conditions were considered too small to affect the fan acoustic performance.

**14. SUBJECT TERMS**

Wind tunnel; Wind tunnel model; Powered model; Scale model; Turbofan; Fan; Rotor alone; Vane; Outlet guide vane; Ducted fan; Fan blade; Stator; Turbomachinery; Performance; Efficiency; Fan noise

**15. NUMBER OF PAGES**

29

**16. PRICE CODE**

| 17. SECURITY CLASSIFICATION OF REPORT | 18. SECURITY CLASSIFICATION OF THIS PAGE | 19. SECURITY CLASSIFICATION OF ABSTRACT | 20. LIMITATION OF ABSTRACT |
|---|---|---|---|
| Unclassified | Unclassified | Unclassified | |